



A model for the 77 K excited state dynamics in *Chlamydomonas reinhardtii* in state 1 and state 2



Joris J. Snellenburg, Lucyna M. Wlodarczyk, Jan P. Dekker, Rienk van Grondelle, Ivo H.M. van Stokkum *

Institute for Lasers, Life and Biophotonics, Faculty of Sciences, Vrije Universiteit Amsterdam, De Boelelaan 1081, 1081, HV, Amsterdam, The Netherlands

ARTICLE INFO

Article history:

Received 2 August 2016

Received in revised form 6 October 2016

Accepted 7 October 2016

Available online 21 October 2016

Keywords:

Chlamydomonas reinhardtii
time-resolved fluorescence
target analysis
77 K

ABSTRACT

The regulatory mechanism of state transitions was studied in *Chlamydomonas reinhardtii* (*C.r.*) wild type (WT) as well as mutant strains deficient in the photosystem I (PSI) or the photosystem II (PSII) core. Time-resolved fluorescence measurements were obtained on instantly frozen cells incubated beforehand in the dark in aerobic or anaerobic conditions which leads to state 1 (S1) or state 2 (S2). WT data contains information on the light-harvesting complex (LHC) connected to PSI and PSII. The mutants' data contain information on either LHCII-LHCI-PSI or LHCII-PSII, plus information on LHC antennas devoid of a PS core. In a simultaneous analysis of the data from all strains under S1 or S2 conditions a unified model for the excited state dynamics at 77 K was created. This yielded the completely resolved LHCII-LHCI-PSI and LHCII-PSII dynamics and quantified the state transitions. In WT cells the fraction of light absorbed by LHCII connected to PSII decreases from 45% in S1 to 29% in S2, while it increases from 0% to 16% for LHCII connected to PSI. Thus $(16/45 =)$ 36% of all LHCII is involved in the state transition. In the mutant strains deficient in the PSI core, the red most species peaking at 716 nm disappears completely, indicating that this far red Chl pigment is located in the PSI core. In the mutant strain deficient in the PSII core, red shifted species with maxima at 684 and 686 nm appear in the LHCII antenna. LHCII-684 is quenched and decays with a rate of $(310 \text{ ps})^{-1}$.

© 2016 Elsevier B.V. All rights reserved.

1. Introduction

The primary processes of photosynthesis take place on the picosecond timescale and involve light absorption by a chromophore, excited state energy transfer to a reaction center (RC) and subsequent charge separation [5,23]. These events occur within the pigment-protein complexes of Photosystem I (PSI) and Photosystem II (PSII) where most of the light is absorbed by the so-called light harvesting complexes bound to the cores of PSI (LHCI) and PSII (LHCII) [2,8,24]. A regulatory mechanism called state transitions exists that balances the excitation energy input between the two photosystems for maximum efficiency of downstream processes [1,6,40,45]. Upon state 1 (S1) to state 2 (S2) transition part of the LHCII antenna functionally connected to PSII disassociates and binds to PSI [15,59]. In the model organism *Chlamydomonas reinhardtii* (*C.r.*) this effect was found to be large [11]. The magnitude and the exact amount of LHCII binding to PSI is debated, and also various amounts of disconnected LHCII are being reported [46,62,65].

In order to quantify the amount and the function of the LHCII involved in state transitions, time-resolved fluorescence spectroscopy is routinely employed [61,62,64,65]. However, with *in vivo* studies, the fluorescence is a superposition of the emissions from all the different pigment-protein complexes embedded in the thylakoid membrane: PSI core, PSII

core, LHCI, and LHCII. Under S1 conditions the supercomplexes LHCI-PSI and LHCII-PSII are found, while under S2 conditions LHCII-LHCI-PSI and disconnected LHCII can occur. Accurate quantification of the energy absorbed by LHCII passing through PSI or PSII requires a detailed model for the dynamics of all of these complexes.

Previously, the so-called functional compartmental modelling was used to characterize the excited state dynamics of the isolated pigment-protein complexes LHCI-PSI and PSII core, as well as of the PSII membranes [53]. 'Functional' means here that the excited state dynamics is resolved in a number of distinct species, each with a specific role (e.g. antenna pigment, bulk Chls, photochemical trapping, red states, etc.). Certainly many other successful examples of compartmental modelling of emission data recorded on isolated photosystems are available, e.g. for (isolated) PSI [19,29,31,32,36,52], and for PSII [17,30,39,41,58].

Studies on mutants lacking either photosystem make it possible to follow/investigate the *in vivo* dynamics of the isolated photosystem within the context of the whole cell [7,60]. This approach is a crucial step towards understanding how the native system (wild type chloroplasts, thylakoids, whole cells, leaves) works. There have been only handful studies on such systems [28,38,60]. Extending the same level of detailed modeling to measurements on whole thylakoids, fully resolving the dynamics of PSI and PSII complexes within the membrane remains a challenge. Intuitively one might expect that a superposition of the models describing the dynamics of isolated PSI and PSII complexes will work well, but one should consider a number of caveats. Firstly,

* Corresponding author.

E-mail addresses: ivo@few.vu.nl, i.h.m.van.stokkum@vu.nl (I.H.M. van Stokkum).

the dynamics of the isolated complexes do not need to be the same as the dynamics within the whole cell, e.g. the isolated complex could be missing loosely coupled subunits. Secondly, simply taking the superposition of two already complex models can add too much freedom in the parameter estimation, resulting in a numerically unstable model. Thirdly, the estimated spectra might show a large degree of mixing of amplitudes (i.e. PSI with characteristics of PSII and vice versa) giving little confidence in the correctness of the model, considering that these estimated spectral shapes are the primary biophysical test for the correctness of the model. One way to handle the increased complexity and deal with these caveats is to analyze two or more datasets simultaneously. By analyzing the time-resolved emission from stacked and unstacked thylakoids [12] simultaneously making use of the difference in excitation transfer from LHCI to the photosystems in the two conditions it was possible to partially resolve the photosystem dynamics [53]. Inspired by this success, the same method was applied to describe and quantify the effect of state transitions induced in *C.r.* [65]. In these studies it was not yet possible to resolve the internal photosystem dynamics as could be done for the isolated photosystems, suggesting that the data obtained on stacked versus unstacked membranes or S1 versus S2 cells by itself are not sufficient to fully resolve the dynamics of both photosystems.

Recently time-resolved fluorescence studies comparing intact cells of *C.r.*, wild type (WT) with *C.r.* strains lacking essential subunits of the PSI core or the PSII core have been published [64]. The intact cells of WT *C.r.*, the PSI-core deficient mutants F15 and M18 and the PSII-core deficient mutant FUD7, were first incubated under conditions promoting either S1 or S2 and then their time-resolved emission was measured at 77 K. WT data contains information on the amount and dynamics of LHC connected to PSI and PSII. The mutants' data contain information on either LHCI-LHCI-PSI or LHCI-PSII, plus information on LHC antennas devoid of a PS core. In a simultaneous analysis of the data from all strains under S1 or S2 conditions a unified model for the excited state dynamics at 77 K was created. In a simultaneous target analysis of all datasets it will be demonstrated that we can now resolve completely resolve the LHCI-LHCI-PSI and LHCI-PSII dynamics in the intact cells of *C.r.* in S1 or S2 conditions.

2. Materials and Methods

The wild type reference strain (*C.r.* WT strain 137c) came from the lab of Prof. Jean-David Rochaix. Mutants F15 (cc-4138), M18 (cc-1051) and FUD7 (cc-4147) originated from the Chlamydomonas Resource Center (University of Minnesota). The direct effect of mutations introduced in F15 and in M18 is the lack of respectively PsaB and PsaA protein [18,54], while FUD7 is devoid of the D1 protein [66]. Growth conditions, treatments and measurement protocols have been described in more detail before [64]. Briefly, the cells were grown in TAP medium [22] at 25 °C in dim light (< 5 μ E) on an incubator shaker (Minitron, INFORS HT). The cells were either incubated in dark under S1 conditions (aeration), or under S2 conditions (bubbling with N₂) for 45 min before they had been instantly frozen and kept at 77 K for the duration of the measurements. The samples were measured by [64] on a synchroscan streak-camera setup described in detail elsewhere [55,57]. The excitation pulses (400 nm, \approx 100 fs) carried an energy per pulse of approximately 1 nJ and were used to excite the sample with a repetition rate of 250 kHz. Time-resolved emission in the window of 660 nm to 818 nm over a range of 1.5 ns with 1.5 ps step size was used for data analysis. The full width at half maximum (FWHM) of the instrument response function (IRF) was estimated from the data and found to be 22 ps.

2.1. Compartmental modelling and global analysis

The ultrafast dynamics in photosynthetic systems is modelled as a system of coupled differential equations (ODEs), called a

compartmental model [20], where the compartments correspond to functional states in the assembly of pigment-protein complexes. In general, these states possess unknown spectra, and from the measured time-resolved spectra of the system one must solve the inverse problem: find an appropriate biophysical model, and estimate the kinetic and spectral parameters, in the form of rate constants and species-associated spectra (SAS). These SAS and their dynamic properties may then lead us to the underlying molecular states and dynamics of each compartment. The modelling of time-resolved spectroscopic data using compartmental models has been described in great detail elsewhere [4,26,27,56]. The parameter estimation is based upon a nonlinear least squares analysis, in combination with the efficient partitioned variable projection algorithm [21,43,44]. We use constraints of equal SASs' area to estimate equilibria between species as described in [53].

2.2. Simultaneous target analysis

Target analysis is a powerful method to analyze a single time-resolved measurement, but the real advantage is revealed when multiple measurements are fitted simultaneously. The challenge therein is to find the appropriate biophysical model that applies to all measurements simultaneously and estimate the kinetic and spectral parameters within a shared parameter space. Simultaneously fitting multiple datasets in which different aspects of the complete photosystem dynamics can be more easily resolved is a way to solve the complete system. This is where the role of the different mutants becomes clear. Although *C.r.* WT will contain information on the dynamics of LHCI-PSI as well as LHCI-PSII, these contributions are hard to separate. But the FUD7 mutant is deficient in the PSII core, thus mainly LHCI-PSI and the remaining LHCI antenna are expected to contribute, with possible minor contribution of CP43/CP47. On the other hand the F15 and M18 mutants are deficient in the PSI core, thus only LHCI-PSII, remaining LHCI antenna and possibly uncoupled LHCI complexes are expected to contribute. All strains were studied upon incubation to either S1 or S2 which we know from earlier work aids in resolving the WT dynamics of PSI and PSII [65], and is also relevant for the mutants deficient in either photosystem [64]. This means that we might also expect additional contributions from the interaction of the LHCI complex and the photosystems (or what remains), e.g. from LHCI-LHCI-PSI and LHCI-LHCI. This leads us to propose the simultaneous target analysis scheme in Fig. 1. The colored boxes indicate the different subunits of the model: LHCI-PSI (blue), LHCI-PSII (red), LHCI (orange), LHCI (purple), and mobile LHCI (light red). Whether the mobile LHCI binds to form supercomplexes or is disconnected is investigated in the modeling. The internal excited state dynamics of a subunit is not relevant at this level but is discussed in detail in the Results section. The possible electronic coupling between subunits and the assumption that in the mutants the remaining photosystem's dynamics is unaffected is also investigated in the modelling.

The analysis scheme as depicted in Fig. 1 would hold regardless of whether the measurements were done at room temperature or 77 K. But the kinetics (and spectral properties) of each subunit (e.g. the photosystem dynamics) is temperature dependent because uphill energy transfer slows down with decreasing temperature according to the Boltzmann distribution.

In this work we will only report on measurements obtained at 77 K, where the low lying energy states in PSI contribute most. An increase in the amount of LHCI connected to LHCI-PSI caused by the state transition is then more easily detected. For each subunit of the model the internal dynamics will be reported.

3. Results

Here we present the results of a simultaneous analysis of eight time-resolved fluorescence measurements at 77 K from [64] on four different

Simultaneous target analysis scheme

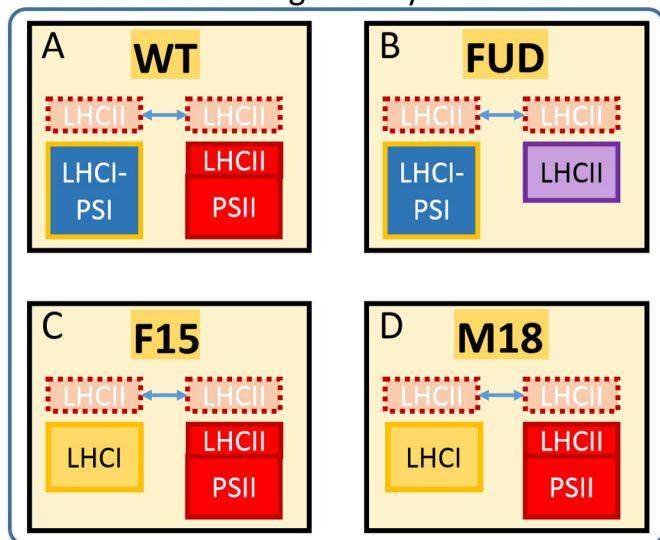


Fig. 1. Simultaneous target analysis scheme to model the time-resolved fluorescence recorded on whole cells of *Chlamydomonas reinhardtii* WT and the mutants FUD7, F15 and M18 incubated under S1 or S2 conditions. The dashed LHCII boxes and the blue arrows indicate a fraction of mobile LHCII antenna, which when bound results in the supercomplexes LHCII-LHCI-PSI and LHCII-LHCI, as well as LHCII-PSII and LHCII with a variable amount of LHCII.

strains of whole cell *C.r.* (WT, the strains F15 and M18 that lack the PSII core complex and the strain FUD7 that lacks the PSII core complex), each incubated under S1 (by bubbling for 45 min in the dark in air) or under S2 conditions (by bubbling for 45 min in the dark in N_2). For a biochemical analysis of the investigated WT and mutant cells as well as for steady-state emission spectra at 77 K and a global analysis of the time-resolved fluorescence measurements at 77 K we refer to [64]. We also note that the properties of the states S1 and S2 could be different from those obtained by other treatments, and stress that quantitative predictions of state transition only apply to the specific protocols used here and that the methodology that we develop in this paper could also be applied to states obtained by different pretreatments. The results of the simultaneous analysis of all eight measurements are schematically depicted in Fig. 1.

3.1. The five subunits of the compartmental model

We will first discuss the results for each subunit of the compartmental model in detail and show the estimated dynamics and corresponding SAS for the most representative sample (the dataset where its contribution is most pronounced). The four static subunits are discussed in separate subchapters below, the relation between the fifth (the mobile LHCII subunit) and each of the four static subunits is discussed in these subchapters. Ultimately we combine these different subunits into the full compartmental model that is used for the simultaneous analysis of all eight datasets.

3.1.1. LHCII-PSII supercomplex

The first subunit of the compartmental model describes the excited state dynamics of the LHCII-PSII supercomplex. It applies to the measurements on the *C.r.* WT, F15 and M18, each incubated under S1 or S2 conditions. This subunit consists of 5 compartments, of which two can be assigned to LHCII dynamics (LHCII-676, LHCII-681) and three to the dynamics of the PSII core (PSII-684, PSII-690 and PSII-695). The compartmental model for this subunit together with the population dynamics for WT and the estimated spectra are shown in Fig. 2.

From the population dynamics in Fig. 2B it can be seen that the dominant contribution in the first 500 ps of the measurement comes

from the PSII-684 (red) compartment, which contains the bulk Chl *a* in the PSII core and the reaction center (RC). Its SAS has a peak emission peaking around 684 nm and a vibrational tail extending up to 780 nm (Fig. 2C). From this compartment quenching takes place with a rate Q . We do not discuss the mechanism of quenching here, the quenching can be either non-photochemical or photochemical, as proposed before [3]. The PSII-684 compartment would be the main contributor to the F-685 fluorescence of PSII measured at 77 K under steady-state conditions. From the present data it can be seen that the variable quenching rate Q depends on the *C.r.* strain and its state (S1 vs S2). In another paper, Włodarczyk et al. (in preparation) have used this target model to investigate how these quenching rates change as a function of light exposure.

PSII-684 is in equilibrium with two compartments representing lower lying energy states with peak emission at 690 nm (PSII-690, blue) and 695 nm (PSII-695, turquoise). The PSII-690 compartment represents a relatively shallow trap from which excitation energy can still escape to the bulk (as represented by a relatively large back rate of 2.4 ns^{-1} versus the forward rate of 1.3 ns^{-1}). The PSII-695 compartment represents a deep trap from which the excitation energy only disappears with an estimated intrinsic fluorescence decay rate of 0.2 ns^{-1} . These characteristics are consistent with a relatively shallow and a deep trap in the CP47 complex [3,9,13,33].

PSII-684 is partly excited directly, and partly populated via the energy transfer from the LHCII complex. LHCII is modelled as two compartments in equilibrium: LHCII-676 (light gray), which has a main band around 676 nm, consistent with an assignment to emission from Chl *b* and blue Chl *a*, and LHCII-681 (black), which has a well-defined band at 681 nm, consistent with an assignment to the emission from more red Chl *a* in LHCII. In addition to the main band, both LHCII SAS exhibit amplitude in the region between 735 nm and 750 nm where the contribution from a vibrational sideband is expected [51], in accordance with observations on LHCII emission spectra [50]. Both compartments are fully equilibrated in about 4–5 ps, consistent with the slowest equilibration time scale found in [48,49]. The gray SAS (LHCII-676) is the most difficult to estimate because of its low population and its presence being limited to early times. The equilibration between LHCII and the PSII core takes several tens of picoseconds. The forward rates between the LHCII-681 compartment and the PSII-684 compartment are state transition dependent, in S1 the antenna is larger, resulting in a slower equilibration than in S2. The input into LHCII-676 and LHCII-681 decreases from 45% in S1 to 29% in S2, resulting in a lower population of the PSII related species (dashed lines in Fig. 2).

3.1.2. LHCII in the PSII core deficient mutant

The second subunit contains the excited state dynamics of what remains of LHCII-PSII in the PSII-core deficient mutant FUD7 (the compartment LHCII in purple in Fig. 1). Thus, mainly major and minor light harvesting complexes contribute here. Additionally, the mutant cells were incubated under S1 or S2 conditions. This subunit is largely identical to the LHCII complex in WT, F15 and M18, but with the following changes: (1) there is no connection to a PSII bulk compartment, (2) two additional lower lying states are observed with peak emissions at 684 nm (LHCII-684, purple) and 686 nm (LHCII-686, brown). The lower lying states apparently only become observable when there is no efficient energy transfer possible to a photosystem. The compartmental model for the LHCII + subunit together with its population dynamics and estimated spectra is shown in Fig. 3.

Excitations disappear from the LHCII-684 compartment much faster than in LHCII-686 ($Q = 3.2 \text{ ns}^{-1}$ vs the estimated intrinsic fluorescence rate of 0.2 ns^{-1}) indicating that the former compartment is quenched. This rate of quenching corresponds to a lifetime of around 310 ps. The SAS of LHCII-684 (purple) is most difficult to estimate, it shows a sideband around 710 nm, which could be due to interference with some PSI decay on that same time scale or to red-shifted LHCII emission observed for instance in LHCII aggregates at 77 K and in single-molecule

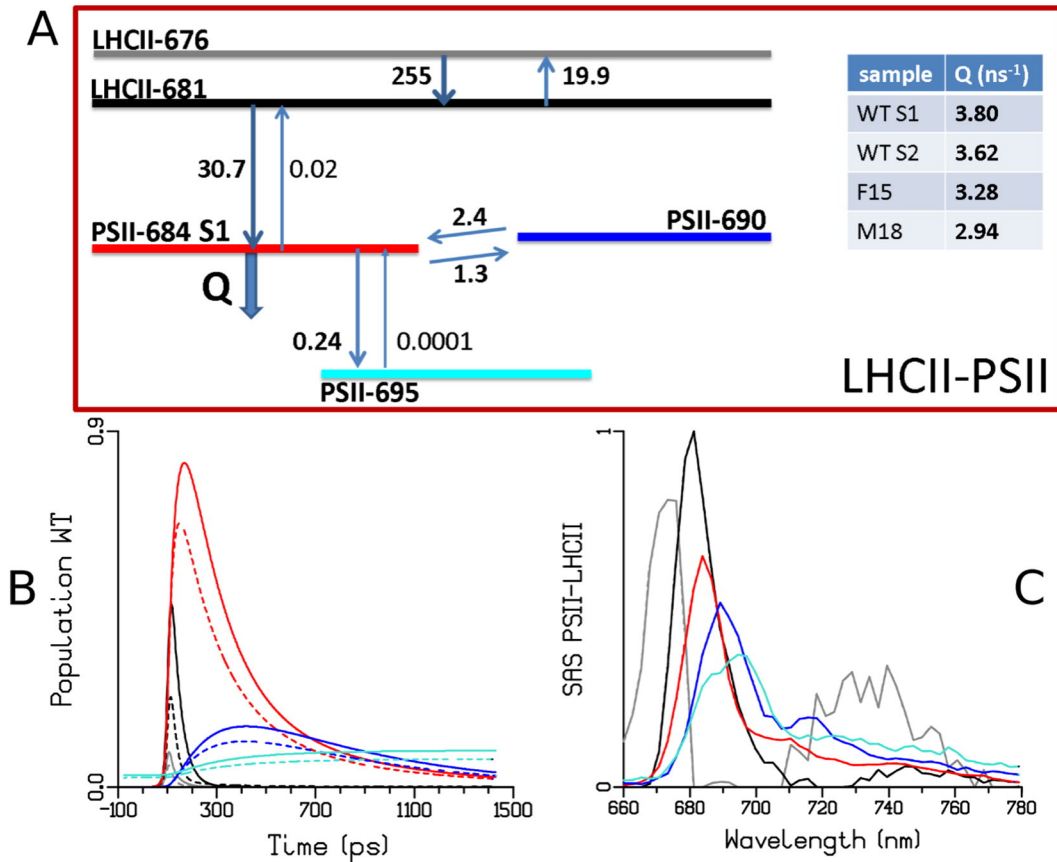


Fig. 2. A) Compartmental model for the LHCII-PSII supercomplex in S1 at 77 K, with estimated rates in ns⁻¹. The variable quenching rate Q is depicted in the inset table. The natural decay rate of 0.2 ns⁻¹ for all compartments has been omitted for clarity. In S2, due to a smaller antenna pool, the forward and backward rates for the equilibrium of LHCII-681 and PSII-684 speed up to 55 and 0.9 ns⁻¹. Rates depicted in bold have a standard error smaller than 10%. B) Population dynamics in WT (S1 solid, S2 dashed) and C) estimated SAS. Key to A-C: LHCII-676 (light gray), LHCII-681 (black), PSII-684 (red), (PSII-690, blue), 695 nm (PSII-695, turquoise).

fluorescence experiments [34,35]. The SAS of LHCII-686 (brown) shows a broad peak and a normal vibrational tail. The effect of the state transition is a decrease of the absorption of LHCII + from 43% to 31%, which leads to an increase in the absorption of LHCII connected to LHCI-PSI (see the next section) from 2% to 14% (cf. Table 1).

3.1.3. LHCI-PSI and LHCII-LHCI-PSI supercomplexes

The third subunit contains the excited state dynamics of LHCI-PSI and LHCII-LHCI-PSI present in WT and FUD7, which we collectively refer to as LHCII-LHCI-PSI (Fig. 4). The LHCI-PSI supercomplex can be modeled as a LHCII-LHCI-PSI supercomplex, where the free parameter representing the absorption by LHCII connected to LHCI-PSI is then estimated to be practically zero. This is the case in S1 as can be seen from the absence of a solid gray and black concentration profile in Fig. 4B. The LHCII compartments, relevant in S2, have the same properties as in LHCII-PSII supercomplexes (cf. Fig. 2). As can be seen in Fig. 4A the LHCII-681 compartment is in equilibrium with the bulk PSI compartment (PSI-694, orange) but the energy flow is largely unidirectional from LHCII to PSI. The rate from LHCII-681 to PSI-694 coincides with that estimated in an isolated LHCII-LHCI-PSI particle [36]. PSI-694 is efficiently quenched photochemically yielding an effective trapping rate of 26 ns⁻¹. There are three compartments functionally representing chlorophylls that are lower in energy than the bulk (typically referred to as red chlorophylls): LHCI-702 (cyan), LHCI-713 (green) and LHCI-716 (magenta), with a peak emission around 702 nm, 713 nm and 716 nm respectively. All three compartments are in equilibrium with the bulk which still allows excitations to escape from these lower energy states, even at 77 K. In

addition to this, these states are only observed to decay via an estimated intrinsic fluorescence decay rate of 0.3 ns⁻¹, slightly higher than in the case of PSII and LHCII. A higher probability of de-trapping (compare the back transfer rates in Fig. 4A with the intrinsic rate of decay) contributes to a relatively long lived presence of the PSI bulk emission despite the fast photochemical trapping rate of 26 ns⁻¹. This can be seen in the concentration profile in Fig. 4B for this species. Note that in this system it cannot be resolved which compartments represent a functional state in the LHCI antenna or in the PSI core, hence the prefix PSI- is used for all LHCI-PSI related states. All PSI SAS have a normal Chl *a* character; PSI-694 is relatively broad with long tails consistent with the energetic distribution over a large number of energetically disordered pigments [16,25]. Because of its long lifetime, the steady-state contribution from the system is largely determined by the emission from PSI-716.

A key finding here is that in WT S1 the absorption of LHCII connected to LHCI-PSI is estimated to be practically zero. In S2 however, the absorption of LHCII coupled to LHCI-PSI increases from 0% to 16% out of the total, concomitant with the decrease of input into LHCII coupled to PSII from 45% to 29% (cf. Fig. 4). Because the direct input into PSI remains unchanged between S1 and S2, due to the additional input received from LHCII, the population dynamics shows a clear increase in PSI related species for S2 (cf. Fig. 4B). Below these results will be discussed in the context of the literature.

3.1.4. LHCI and LHCII-LHCI in the PSI core deficient mutants

The last subunit contains the excited state dynamics of what remains of PSI-LHCI in the PSI-core deficient mutants F15 and M18, consisting of

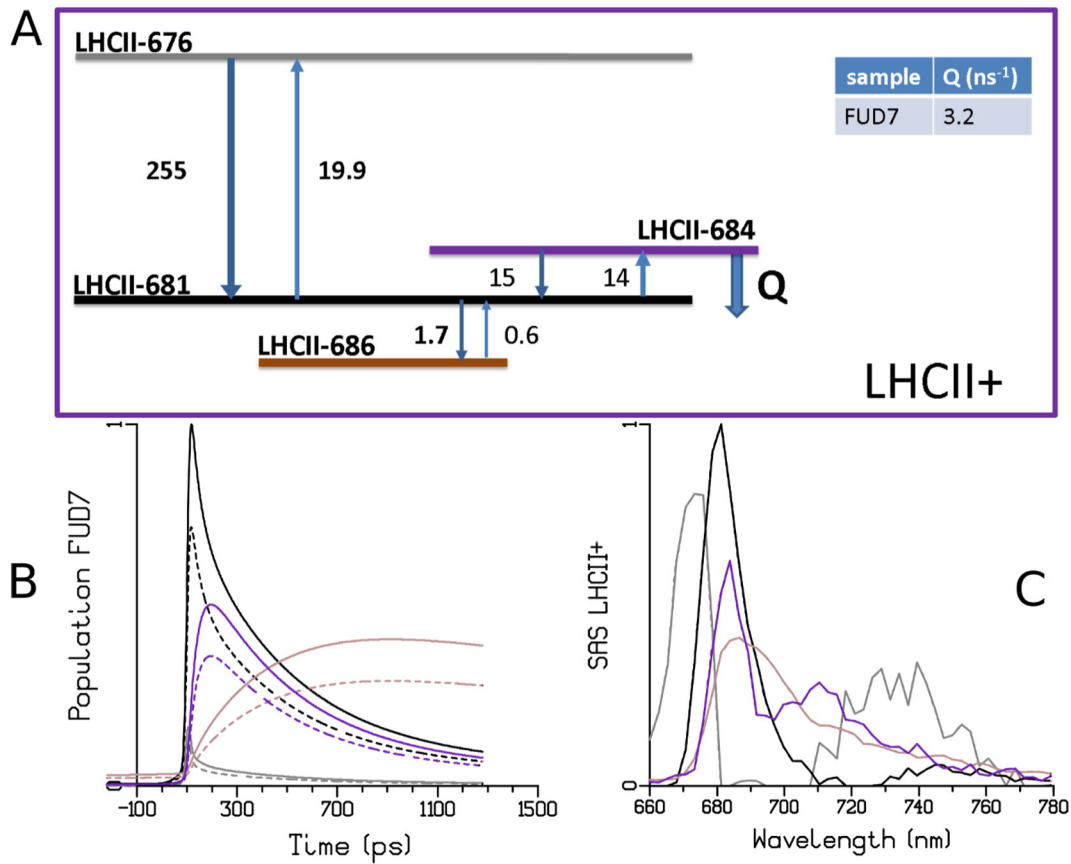


Fig. 3. A) Compartmental model for the LHCII+ subunit present in the PSII core deficient mutant FUD7 at 77 K, with estimated rates in ns^{-1} . The quenching rate Q is depicted in the inset table. The natural decay rate of 0.2 ns^{-1} for all excited state compartments has been omitted for clarity. Rates depicted in bold have a standard error smaller than 10%. B) Population dynamics (S1 solid, S2 dashed) and C) estimated SAS. Key to A-C: LHCII-676 (light gray), LHCII-681 (black), LHCII-684 (purple), LHCII-686 (brown).

LHCI antenna that must be somewhere in the membranes and is possibly connected to LHCII. The compartmental model for the (LHCII-)LHCI supercomplex is shown in Fig. 5. It differs from that in Fig. 4 in the following aspects: (1) there is no trapping or quenching from the bulk compartment, just intrinsic fluorescence decay (0.3 ns^{-1}), (2) there are only two instead of three additional states needed in equilibrium with the bulk (cyan and green) and the equilibration rates are much smaller. Notably PSI-716 is missing, indicating that this relatively deep trap is located in the missing PSI core, an important observation which will be discussed below. Due to the absence of photochemical quenching the population dynamics are significantly slowed down; PSI-713 (green) is not even observed to decay in the measurement window. Also the LHCII-LHCI supercomplex features a clear state transition. In the transition from S1 to S2 the amount of light absorbed by LHCII

connected to LHCI increased from 14.6% to 33.6% for F15 and from 28.2% to 37.8% for M18.

3.2. Synthesis

The full compartmental model that was used for the simultaneous analysis of all eight datasets can now be synthesized following the design of Fig. 1, from the compartmental models of the subunits plus the estimates of the initial excitation input into the relevant compartments. We used a constraint that the total amount of light absorbed by LHCII was the same in S1 and S2. The state transition is quantified by the difference of the distribution of this LHCII between S1 and S2. In WT, there were thus four free fitting parameters for the input: the fraction of light absorbed by LHCI-PSI, PSII, and LHCII to PSI in S1 or S2. The fourth fraction, LHCII to PSII in S1 or S2, is 100% minus the other three fractions. For each of the samples, Table 1 quantifies how much population is present directly after excitation on the LHCI-PSI/LHCI bulk, the PSII bulk and the different LHCII compartments, which is a proxy for the 400 nm absorption cross section of a specific compartment.

Direct excitation into the various red Chl states is neglected because it is assumed that these consist of a small number of pigments which in our experiment absorb relatively little compared to all the pigments in the bulk and LHCII antenna compartments, but which might be functional in increasing the relative cross section under certain in vivo conditions.

In our target model we have not yet attempted to independently estimate the equilibrium between a photosystem and the LHCII-681 compartment connected to it. Instead, we have estimated an average rate for all four samples. With one exception, the microscopic rate constants did not differ between S1 and S2, cf. Fig. S 4 - Fig. S 7. Only

Table 1

Population directly after 400 nm excitation per subunit of the full compartmental model. From the light absorbed by LHCII 54% is absorbed by LHCII-676 and 46% by LHCII-681. *Results from analysis of 475 nm excitation data of [65] reported and explained in the SI.

Sample	LHCI-PSI	LHCI	LHCII to PSI	LHCII to LHCI	LHCII to LHCII	LHCII to PSII	PSII
WT S1	39.5%		0.0%			44.9%	15.6%
WT S2	39.5%		16.1%			28.8%	15.6%
FUD7 S1	54.7%		1.9%		43.4%		
FUD7 S2	54.7%		14.3%		31.0%		
F15 S1		13.3%		14.6%		52.4%	19.7%
F15 S2		13.3%		33.6%		33.4%	19.7%
M18 S1		14.9%		28.2%		33.5%	23.4%
M18 S2		14.9%		37.8%		23.8%	23.4%
WT S1c*	25.2%		0.0%			64.8%	10.0%
WT S2c*	25.2%		26.0%			38.8%	10.0%

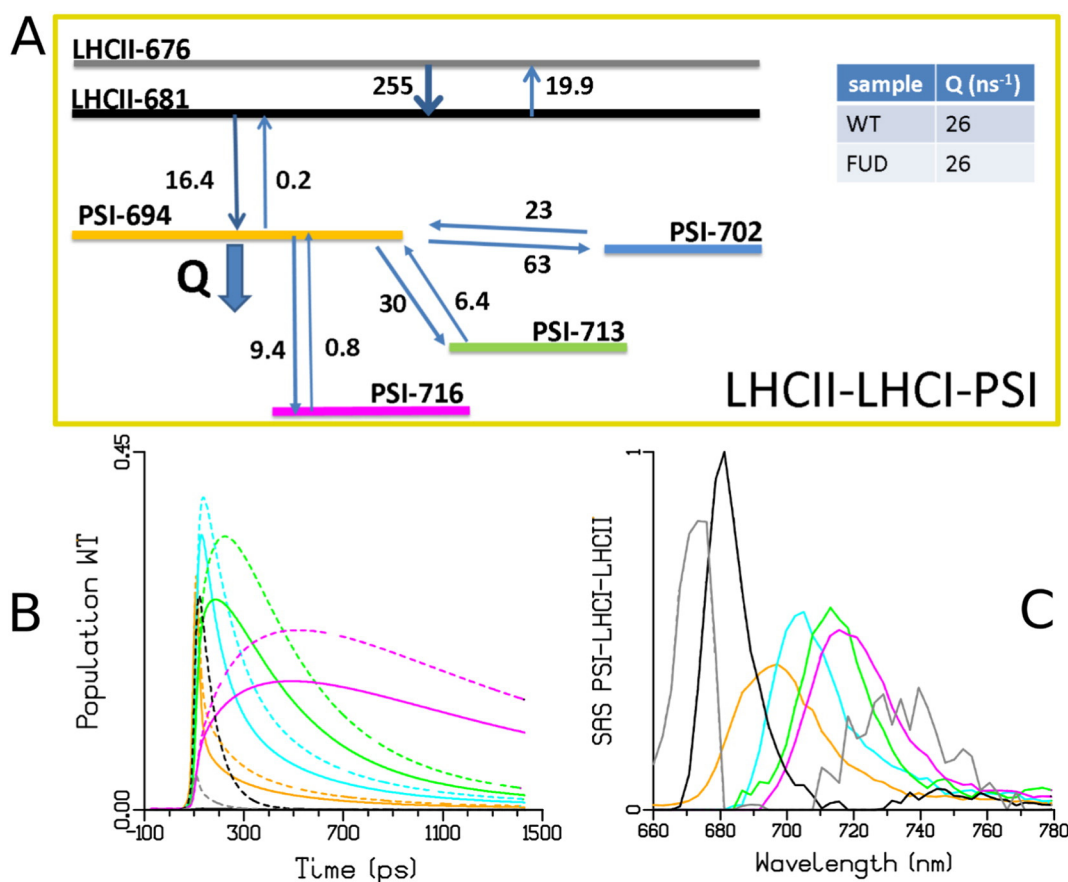


Fig. 4. A) Compartmental model for the LHCII-LHCI-PSI subunit present in WT and FUD7, with estimated rates in ns^{-1} . The rate of photochemical trapping due to charge separation, represented by Q , was fixed to $26/\text{ns}$. The natural decay rates estimated to be 0.3 ns^{-1} for all LHCI and PSI related excited state compartments and 0.2 ns^{-1} for the LHCII related compartments have been omitted for clarity. Rates depicted in bold have a standard error smaller than 10%. B) Population dynamics (S1 solid, S2 dashed) and C) estimated SAS. Key to A-C: LHCII-676 (light gray), LHCII-681 (black), PSI-694 (orange), LHCI-702 (cyan), LHCI-713 (green), LHCI-716 (magenta),

the equilibrium between PSII-684 and the LHCII-681 compartment connected to it differs between S1 and S2. To study for each of the samples the equilibrium between a photosystem and the LHCII-681 compartment connected to it systematic measurements at multiple temperatures are necessary.

Based upon our target model, in FUD7 we find a large fraction of disconnected LHCII (LHCII to LHCII in Table 1). The dynamics as reported in Fig. 3 reveal that this fraction is partially quenched. Upon transitions from S1 to S2 this fraction (of total light absorbed) decreases from 43.4% to 31.0% while the fraction of LHCII connected to PSI increases from 1.9% to 14.3%.

Both F15 and M18 feature a fraction of disconnected LHCI (13.3% and 14.9% respectively) which does not change as a result of inducing the state transition. In addition, both F15 and M18 feature a fraction of LHCII which is connected to this LHCI. In F15 this fraction increases from 14.6% in S1 to 33.6% in S2 and for M18 this fraction increases respectively from 28.2% to 37.8%. In both cases a concomitant change in absorption of LHCII connected to PSII is observed. In general the ratio of antenna to PSII core in F15 is larger than M18, consistent with biochemical characterizations [64].

For WT we find that the fraction of light absorbed by LHCII connected to PSII decreases from 45% in S1 to 29% in S2, while it increases from 0% to 16% for LHCII connected to PSI (Fig. 6). Thus $(16/45 =)$ 36% of all LHCII is involved in the state transition.

In previous work we reported a larger state transition effect and the formation of a pool of disconnected LHCII, when cells were chemically locked in S1 or S2 [65]. With the current set of measurements we find no fraction of disconnected LHCII in WT. To investigate this discrepancy we demonstrate here that the data of the chemically induced state

transition from the 2015 paper can also be described with our current target model, and have included the key results in the bottom rows of Table 1. We can now estimate that the state transition in these data involves $(26.0/64.8 =)$ 40% of all LHCII. For the complete analysis, including the estimated SAS, the fitted traces and residual analysis we refer the reader to the SI. On the basis of the residual analysis (Fig. S 12) we cannot exclude that there was a small fraction of uncoupled LHCII present in the chemically locked S2 giving rise to emission around 685 nm.

4. Discussion

Over the past 30 years different techniques have been used to quantify the effect of the state transition in *C.r.*, in terms of the increase in the cross section of PSI upon state transition and sometimes also in terms of the decrease in the cross section of PSII or the formation of a pool of disconnected LHCII. In 1985 absorption spectroscopy was used to determine an increase of the optical cross-section for PSI in S2 of 50% [10]. In 1996 a photoacoustic technique was employed to determine a similar 50–60% increase in PSI cross section, which was then estimated involved 80% of all LHCII [11], nowadays a highly cited number. In view of the current knowledge on PSII-LHCII composition [15] and PSI-LHCI composition [14] a 50% increase in PSI cross section in S2 would rather translate into approximately 50% of the LHCII antenna involved in the state transition. More recently a combination of circular dichroism and absorption spectroscopy was used to quantify the enhancement of PSI antenna size during state transition at $\approx 20\%$, whereas the decrease in PSII antenna size was estimated at $\approx 70\%$, leading to the conclusion that a large part of LHCII would not bind to PSI [46]. A recent study using time-resolved spectroscopy at room temperature quantified the

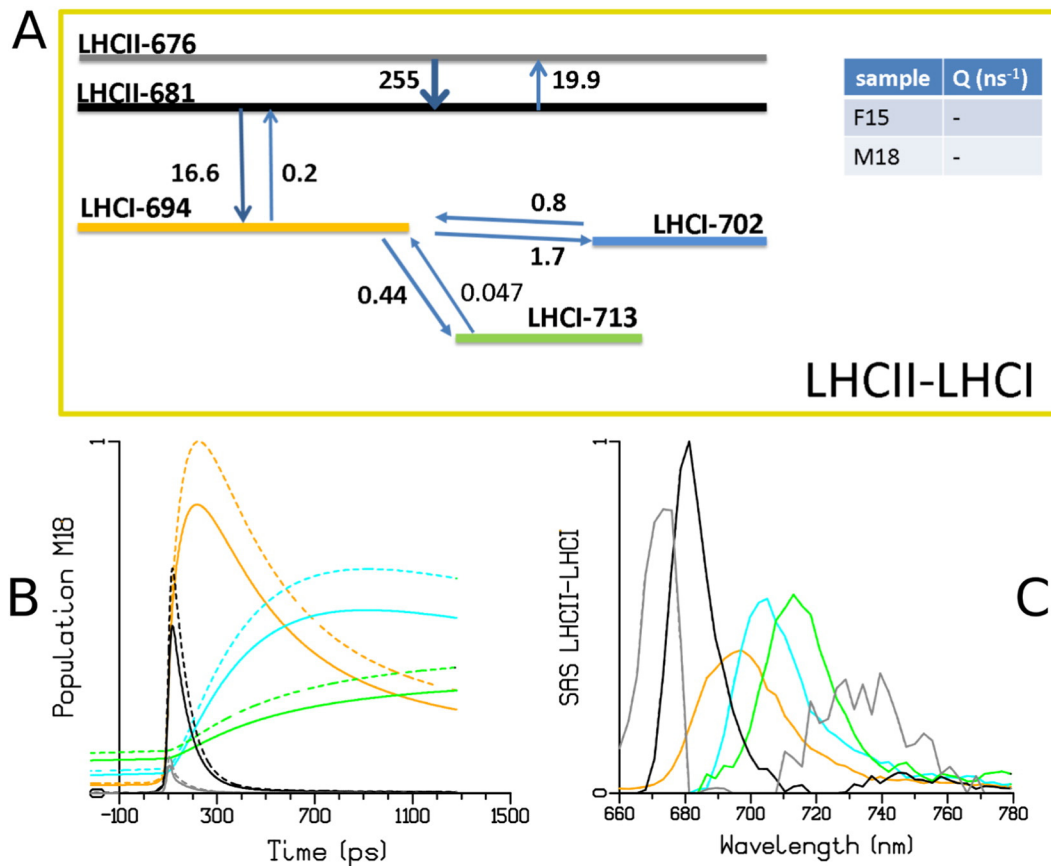


Fig. 5. A) Compartmental model for the LHCII-LHCI complex present in the F15 and M18 mutants, with estimated rates in ns⁻¹. B) Population dynamics in M18 (S1 solid, S2 dashed) and C) estimated SAS. The population profiles of F15 are very similar. The natural decay rates of 0.2 ns⁻¹ for the LHCII and 0.3 ns⁻¹ for the LHCI excited state compartments have been omitted for clarity. Rates depicted in bold have a standard error smaller than 10%. Key to A-C: LHCII-676 (light gray), LHCII-681 (black), PSI-694 (orange), LHCI-702 (cyan), LHCI-713 (green).

increase in PSI at only $\approx 4\%$ [61], which was estimated to involve less than one LHCII trimer on average ($< 10\%$). In addition a substantial fraction of LHCII was found to be functionally detached from PSII. A later study used time-resolved fluorescence spectroscopy at 77 K to arrive at the same conclusion, that the amount of LHC moving from PSII to PSI upon going from S1 to S2 is rather limited [63]. In contrast, another publication using the electrochromic shift method to assess the relative cross section of PSII and PSI arrived at an increase in PSI antenna size of $35 \pm 9\%$, while the decrease in PSII antenna size was estimated at $42 \pm 6\%$ by determining changes in F_{\max} [47]. In their SI these authors provide some explanation for the discrepancy with their results and those reported by ([46,61].

The different experimental methodologies and different methods of quantification of the state transition make a literature review challenging. Not in the least because the extent of the state transition was also found to depend on the way that the state transition was induced (chemically

or non-chemically) and how the cells were locked in either state [65]. However, with our current model we are able to exactly quantify the extent of the state transition in WT *C.r.* and assign changes in PSI or PSII cross section directly to the attached LHCII antenna. Thereby a simultaneous target analysis of the S1 and S2 data is essential. Combined with our experimental methodology of non-chemical induction of state transitions and instantly freezing the intact cells the target model allowed us to quantify the state transition for WT and for the mutant strains deficient in PSI core or PSII core as reported in Table 1. For WT we find an involvement of 36% of LHCII in the state transition as summarized in Fig. 6, which is in agreement with the numbers reported by [47].

To quantify the state transition in *C.r.* using time-resolved spectroscopy we had to develop a detailed model of the excited state dynamics at 77 K, using a simultaneous target analysis of eight measurements on WT and mutant strains. A key finding resulting from this simultaneous target analysis is the missing PSI-716 from the PSI-minus mutants, indicating that the fluorescence from this component originates from the PSI core. This is in agreement with the observation that in mutants lacking the red-most antenna complexes Lhca2 and Lhca9 the main 77 K steady state emission band, peaking at 716 nm hardly changes [14,37,42].

Conflict of interest

The authors declare that they have no conflict of interest.

Author Contributions

The manuscript was written through contributions of all authors. All authors have given approval to the final version of the manuscript.

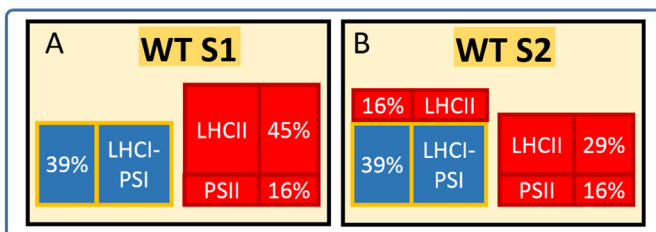


Fig. 6. Simultaneous analysis scheme indicating the fraction of light absorbed for WT S1 (A) and S2 (B). Upon S1 to S2 transition 36% of the total LHCII population functionally associated with PSI, while the population functionally connected to PSII decreased with the same amount.

Abbreviations

Chl	Chlorophyll
PSI	Photosystem I
PSII	Photosystem II
RC	Reaction Center
SAS	Species Associated Spectrum

Transparency document

The Transparency document associated with this article can be found, in the online version.

Acknowledgment

Roberta Croce and Bart van Oort are thanked for helpful discussion. This project was carried out in part within the research programme of BioSolar Cells, co-financed by the Dutch Ministry of Economic Affairs (JJS, JD, RvG, and IHMV). RvG and IHMV acknowledge financial support of the European Research Council (Advanced Grant proposal 267333 (PHOTPROT) to RvG). RvG gratefully acknowledges his Academy Professorship from the Netherlands Royal Academy of Sciences (KNAW) and his support from the Canadian Institute For Advanced Research (CIFAR).

Appendix A. Supplementary data

Supplementary data to this article can be found online at doi:10.1016/j.bbabo.2016.10.001.

References

- [1] J.F. Allen, State transitions—a question of balance, *Science* 299 (5612) (2003) 1530–1532.
- [2] H. van Amerongen, R. Croce, Light harvesting in photosystem II, *Photosynth. Res.* 116 (2–3) (2013) 251–263.
- [3] E.G. Andrizhivskaya, A. Chojnicka, J.A. Bautista, B.A. Diner, R. van Grondelle, J.P. Dekker, Origin of the F685 and F695 fluorescence in photosystem II, *Photosynth. Res.* 84 (1–3) (2005) 173–180.
- [4] J.M. Beechem, E. Gratton, M. Ameloot, J.R. Knutson, L. Brand, The global analysis of fluorescence intensity and anisotropy decay data: second-generation theory and programs, *Topics in fluorescence spectroscopy*, Springer 2002, pp. 241–305.
- [5] R.E. Blankenship, *Molecular Mechanisms of Photosynthesis*, Wiley, 2014.
- [6] C. Bonaventura, J. Myers, Fluorescence and oxygen evolution from *Chlorella pyrenoidosa*, *Biochim. Biophys. Acta Bioenerg.* 189 (3) (1969) 366–383.
- [7] V.V. Chukhutsina, L. Tian, G. Ajlani, H. van Amerongen, Time-Resolved Fluorescence of Photosystem I in Vivo: Global and Target Analysis, *Photosynthesis Research for Food, Fuel and the Future*, Springer 2013, pp. 465–468.
- [8] R. Croce, H. van Amerongen, Light-harvesting in photosystem I, *Photosynth. Res.* 116 (2–3) (2013) 153–166.
- [9] F.L. de Weerd, M.A. Palacios, E.G. Andrizhivskaya, J.P. Dekker, R. van Grondelle, Identifying the lowest electronic states of the chlorophylls in the CP47 core antenna protein of photosystem II, *Biochemistry* 41 (51) (2002) 15224–15233.
- [10] P. Delepelaire, F.-A. Wollman, Correlations between fluorescence and phosphorylation changes in thylakoid membranes of *Chlamydomonas reinhardtii* in vivo: a kinetic analysis, *Biochim. Biophys. Acta Bioenerg.* 809 (2) (1985) 277–283.
- [11] R. Delosme, J. Olive, F.-A. Wollman, Changes in light energy distribution upon state transitions: an in vivo photoacoustic study of the wild type and photosynthesis mutants from *Chlamydomonas reinhardtii*, *Biochim. Biophys. Acta Bioenerg.* 1273 (2) (1996) 150–158.
- [12] C.D. van der Weij-de Wit, J.A. Ihalainen, R. van Grondelle, J.P. Dekker, Excitation energy transfer in native and unstacked thylakoid membranes studied by low temperature and ultrafast fluorescence spectroscopy, *Photosynth. Res.* 93 (1–3) (2007) 173–182.
- [13] R.J. van Dorssen, J. Breton, J.J. Plijter, K. Satoh, H.J. van Gorkom, J. Amesz, Spectroscopic properties of the reaction center and of the 47 kDa chlorophyll protein of photosystem II, *Biochim. Biophys. Acta Bioenerg.* 893 (2) (1987) 267–274.
- [14] B. Drop, M. Webber-Birungi, F. Fusetti, R. Kouřil, K.E. Redding, E.J. Boekema, R. Croce, Photosystem I of *Chlamydomonas reinhardtii* contains nine light-harvesting complexes (Lhca) located on one side of the core, *J. Biol. Chem.* 286 (52) (2011) 44878–44887.
- [15] B. Drop, K. Yadav, E.J. Boekema, R. Croce, Consequences of state transitions on the structural and functional organization of photosystem I in the green alga *Chlamydomonas reinhardtii*, *Plant J.* 78 (2) (2014) 181–191.
- [16] A. Freiberg, K. Timpmann, S. Lin, N.W. Woodbury, Exciton relaxation and transfer in the LH2 antenna network of photosynthetic bacteria, *J. Phys. Chem. B* 102 (52) (1998) 10974–10982.
- [17] G. Gatzert, M.G. Muller, K. Griebenow, A.R. Holzwarth, Primary processes and structure of the photosystem II reaction center O3. Kinetic analysis of picosecond energy transfer and charge separation processes in the D1-D2-cyt-b559 complex measured by time-resolved fluorescence, *J. Phys. Chem.* 100 (17) (1996) 7269–7278.
- [18] J. Girard, N.H. Chua, P. Bennoun, G. Schmidt, M. Delosme, Studies on mutants deficient in the photosystem I reaction centers in *Chlamydomonas reinhardtii*, *Curr. Genet.* 2 (3) (1980) 215–221.
- [19] B. Gobets, I.H.M. van Stokkum, M. Rogner, J. Kruij, E. Schlodder, N.V. Karapetyan, J.P. Dekker, R. van Grondelle, Time-resolved fluorescence emission measurements of photosystem I particles of various cyanobacteria: A unified compartmental model, *Biophys. J.* 81 (1) (2001) 407–424.
- [20] K. Godfrey, *Compartmental models and their application*, Academic Press, London, 1983.
- [21] G.H. Golub, R.J. LeVeque, Extensions and uses of the variable projection algorithm for solving nonlinear least squares problems, *Proc. of the 1979 Army Numerical Analysis and Comp. Conf.*, ARO Report 79–3, 1979.
- [22] D.S. Gorman, R. Levine, Cytochrome f and plastocyanin: their sequence in the photosynthetic electron transport chain of *Chlamydomonas reinhardtii*, *Proc. Natl. Acad. Sci.* 54 (6) (1965) 1665–1669.
- [23] R. van Grondelle, Excitation energy transfer, trapping and annihilation in photosynthetic systems, *Biochim. Biophys. Acta Bioenerg.* 811 (2) (1985) 147–195.
- [24] R. van Grondelle, J.P. Dekker, T. Gillbro, V. Sundstrom, Energy transfer and trapping in photosynthesis, *Biochim. Biophys. Acta Bioenerg.* 1187 (1) (1994) 1–65.
- [25] R. van Grondelle, V.I. Novoderezhkin, Energy transfer in photosynthesis: experimental insights and quantitative models, *Phys. Chem. Chem. Phys.* 8 (7) (2006) 793–807.
- [26] C.T. Holcomb, R.S. Knox, The relationship of intercompartmental excitation transfer rate constants to those of an underlying physical model, *Photosynth. Res.* 50 (2) (1996) 117–131.
- [27] A.R. Holzwarth, Data Analysis of Time-Resolved Measurements, in: J. Amesz, A.J. Hoff (Eds.), *Biophysical Techniques in Photosynthesis*, Kluwer, Dordrecht, The Netherlands 1996, pp. 75–92.
- [28] A.R. Holzwarth, Y. Miloslavina, M. Nilkens, P. Jahns, Identification of two quenching sites active in the regulation of photosynthetic light-harvesting studied by time-resolved fluorescence, *Chem. Phys. Lett.* 483 (4) (2009) 262–267.
- [29] A.R. Holzwarth, M.G. Muller, J. Niklas, W. Lubitz, Charge recombination fluorescence in photosystem I reaction centers from *Chlamydomonas reinhardtii*, *J. Phys. Chem. B* 109 (12) (2005) 5903–5911.
- [30] A.R. Holzwarth, M.G. Muller, M. Reus, M. Nowaczyk, J. Sander, M. Rogner, Kinetics and mechanism of electron transfer in intact photosystem II and in the isolated reaction center: Pheophytin is the primary electron acceptor, *Proc. Natl. Acad. Sci. U.S.A.* 103 (18) (2006) 6895–6900.
- [31] A.R. Holzwarth, G. Schatz, H. Brock, E. Bittersmann, Energy-Transfer and Charge Separation Kinetics in Photosystem-I O1. Picosecond Transient Absorption and Fluorescence Study of Cyanobacterial Photosystem-I Particles, *Biophys. J.* 64 (6) (1993) 1813–1826.
- [32] J.A. Ihalainen, I.H.M. van Stokkum, K. Gibasiewicz, M. Germano, R. van Grondelle, J.P. Dekker, Kinetics of excitation trapping in intact Photosystem I of *Chlamydomonas reinhardtii* and *Arabidopsis thaliana*, *Biochim. Biophys. Acta Bioenerg.* 1706 (3) (2005) 267–275.
- [33] M. Komura, Y. Shibata, S. Itoh, A new fluorescence band F689 in photosystem II revealed by picosecond analysis at 4–77 K: Function of two terminal energy sinks F689 and F695 in PS II, *Biochim. Biophys. Acta Bioenerg.* 1757 (12) (2006) 1657–1668.
- [34] T.P.J. Krüger, G. Illoia, M.P. Johnson, A.V. Ruban, R. Van Grondelle, Disentangling the low-energy states of the major light-harvesting complex of plants and their role in photoprotection, *Biochim. Biophys. Acta Bioenerg.* 1837 (7) (2014) 1027–1038.
- [35] T.P.J. Krüger, V.I. Novoderezhkin, C. Illoia, R. van Grondelle, Fluorescence Spectral Dynamics of Single LHClI Trimers, *Biophys. J.* 98 (12) (2010) 3093–3101.
- [36] C. Le Quiniou, B. van Oort, B. Drop, H.M. van Stokkum, R. Croce, The High Efficiency of Photosystem I in the Green Alga *Chlamydomonas reinhardtii* Is Maintained after the Antenna Size Is Substantially Increased by the Association of Light-harvesting Complexes II, *J. Biol. Chem.* 290 (51) (2015) 30587–+.
- [37] C. Le Quiniou, L. Tian, B. Drop, E. Wientjes, I.H. van Stokkum, B. van Oort, R. Croce, PSI-LHCI of *Chlamydomonas reinhardtii*: Increasing the absorption cross section without losing efficiency, *Biochim. Biophys. Acta Bioenerg.* 1847 (4) (2015) 458–467.
- [38] Y. Miloslavina, I. Grouneva, P.H. Lambrev, B. Lepetit, R. Goss, C. Wilhelm, A.R. Holzwarth, Ultrafast fluorescence study on the location and mechanism of non-photochemical quenching in diatoms, *Biochim. Biophys. Acta Bioenerg.* 1787 (10) (2009) 1189–1197.
- [39] Y. Miloslavina, M. Szczepaniak, M.G. Muller, J. Sander, M. Nowaczyk, M. Rogner, A.R. Holzwarth, Charge separation kinetics in intact photosystem II core particles is trap-limited. A picosecond fluorescence study, *Biochemistry* 45 (7) (2006) 2436–2442.
- [40] J. Minagawa, State transitions—the molecular remodeling of photosynthetic supercomplexes that controls energy flow in the chloroplast, *Biochim. Biophys. Acta Bioenerg.* 1807 (8) (2011) 897–905.
- [41] F. van Mourik, M.L. Groot, R. van Grondelle, J.P. Dekker, I.H.M. van Stokkum, Global and target analysis of fluorescence measurements on photosystem 2 reaction centers upon red excitation, *Phys. Chem. Chem. Phys.* 6 (20) (2004) 4820–4824.
- [42] M. Mozzo, M. Mantelli, F. Passarini, S. Caffarri, R. Croce, R. Bassi, Functional analysis of Photosystem I light-harvesting complexes (Lhca) gene products of *Chlamydomonas reinhardtii*, *Biochim. Biophys. Acta Bioenerg.* 1797 (2) (2010) 212–221.

- [43] K.M. Mullen, I.H.M. van Stokkum, The variable projection algorithm in time-resolved spectroscopy, microscopy and mass spectrometry applications, *Numer. Algorithm.* 51 (3) (2009) 319–340.
- [44] K.M. Mullen, I.H.M. van Stokkum, Exponential models for time-resolved spectroscopy data, in: V. Pereyra, G. Scherer (Eds.), *Exponential Data Fitting and its Applications*. Bentham 2010, pp. 110–127.
- [45] N. Murata, Control of excitation transfer in photosynthesis I. Light-induced change of chlorophyll a fluorescence in *Porphyridium cruentum*, *Biochim. Biophys. Acta Bioenerg.* 172 (2) (1969) 242–251.
- [46] G. Nagy, R. Ünneper, O. Zsiros, R. Tokutsu, K. Takizawa, L. Porcar, L. Moyet, D. Petroustos, G. Garab, G. Finazzi, Chloroplast remodeling during state transitions in *Chlamydomonas reinhardtii* as revealed by noninvasive techniques in vivo, *Proc. Natl. Acad. Sci.* 111 (13) (2014) 5042–5047.
- [47] W.J. Nawrocki, S. Santabarbara, L. Mosebach, F.-A. Wollman, F. Rappaport, State transitions redistribute rather than dissipate energy between the two photosystems in *Chlamydomonas*, *Nat. Plants* 2 (2016) 16031.
- [48] V.I. Novoderezhkin, A. Marin, R. van Grondelle, Intra- and inter-monomeric transfers in the light harvesting LHCII complex: the Redfield-Förster picture, *Phys. Chem. Chem. Phys.* 13 (38) (2011) 17093–17103.
- [49] V.I. Novoderezhkin, M.A. Palacios, H. van Amerongen, R. van Grondelle, Excitation dynamics in the LHCII complex of higher plants: modeling based on the 2.72 Å crystal structure, *J. Phys. Chem. B* 109 (20) (2005) 10493–10504.
- [50] M.A. Palacios, F.L. de Weerd, J.A. Ihalainen, R. van Grondelle, H. van Amerongen, Superradiance and exciton (de) localization in light-harvesting complex II from green plants? *J. Phys. Chem. B* 106 (22) (2002) 5782–5787.
- [51] M. Rätsep, J. Linnanto, A. Freiberg, Mirror symmetry and vibrational structure in optical spectra of chlorophyll a, *J. Chem. Phys.* 130 (19) (2009) 194501.
- [52] C. Slavov, M. Ballottari, T. Morosinotto, R. Bassi, A.R. Holzwarth, Trap-Limited Charge Separation Kinetics in Higher Plant Photosystem I Complexes, *Biophys. J.* 94 (9) (2008) 3601–3612.
- [53] J.J. Snellenburg, J.P. Dekker, R. van Grondelle, I.H.M. van Stokkum, Functional Compartmental Modeling of the Photosystems in the Thylakoid Membrane at 77 K, *J. Phys. Chem. B* 117 (38) (2013) 11363–11371.
- [54] O. Stampacchia, J. Girard-Bascou, J.-L. Zanasco, W. Zerges, P. Bennoun, J.-D. Rochaix, A nuclear-encoded function essential for translation of the chloroplast *psaB* mRNA in *Chlamydomonas*, *Plant Cell* 9 (5) (1997) 773–782.
- [55] I.H.M. van Stokkum, B. Gobets, T. Gensch, F. van Mourik, K.J. Hellingwerf, R. van Grondelle, J.T.M. Kennis, (Sub)-picosecond spectral evolution of fluorescence in photoactive proteins studied with a synchroscan streak camera system, *Photochem. Photobiol.* 82 (2) (2006) 380–388.
- [56] I.H.M. van Stokkum, D.S. Larsen, R. van Grondelle, Global and target analysis of time-resolved spectra, *Biochim. Biophys. Acta* 1657 (2004) 82–104.
- [57] I.H.M. van Stokkum, B. van Oort, F. van Mourik, B. Gobets, H. van Amerongen, (Sub)-Picosecond Spectral Evolution of Fluorescence Studied with a Synchroscan Streak-Camera System and Target Analysis, in: T.J. Aartsma, J. Matysik (Eds.), *Biophysical Techniques in Photosynthesis Vol. II, Advances in Photosynthesis and Respiration*, vol. 26, Springer, Dordrecht, The Netherlands 2008, pp. 223–240.
- [58] M. Szczepaniak, J. Sander, M. Nowaczyk, M. Müller, M. Rögner, A. Holzwarth, Charge separation, stabilization, and protein relaxation in photosystem II core particles with closed reaction center, *Biophys. J.* 96 (2) (2009) 621–631.
- [59] H. Takahashi, M. Iwai, Y. Takahashi, J. Minagawa, Identification of the mobile light-harvesting complex II polypeptides for state transitions in *Chlamydomonas reinhardtii*, *Proc. Natl. Acad. Sci. U. S. A.* 103 (2006) 477–482.
- [60] L. Tian, S. Farooq, H. van Amerongen, Probing the picosecond kinetics of the photosystem II core complex in vivo, *Phys. Chem. Chem. Phys.* 15 (9) (2013) 3146–3154.
- [61] C. Ünlü, B. Drop, R. Croce, H. van Amerongen, State transitions in *Chlamydomonas reinhardtii* strongly modulate the functional size of photosystem II but not of photosystem I, *Proc. Natl. Acad. Sci.* 111 (9) (2014) 3460–3465.
- [62] C. Ünlü, I. Polukhina, H. van Amerongen, Origin of pronounced differences in 77 K fluorescence of the green alga *Chlamydomonas reinhardtii* in state 1 and 2, *Eur. Biophys. J.* (2015) 1–9.
- [63] C. Ünlü, I. Polukhina, H. van Amerongen, Origin of pronounced differences in 77 K fluorescence of the green alga *Chlamydomonas reinhardtii* in state 1 and 2, *Eur. Biophys. J.* 45 (3) (2016) 209–217.
- [64] L.M. Włodarczyk, E. Dinc, R. Croce, J.P. Dekker, Excitation energy transfer in *Chlamydomonas reinhardtii* deficient in the PSI core or the PSII core under conditions mimicking state transitions, *Biochim. Biophys. Acta Bioenerg.* 1857 (6) (2016) 625–633.
- [65] L.M. Włodarczyk, J.J. Snellenburg, J.A. Ihalainen, R. van Grondelle, I.H.M. van Stokkum, J.P. Dekker, Functional rearrangement of the light-harvesting antenna upon state transitions in a green alga, *Biophys. J.* 108 (2) (2015) 261–271.
- [66] F.-A. Wollman, C. Lemaire, Studies on kinase-controlled state transitions in photosystem II and *b6f* mutants from *Chlamydomonas reinhardtii* which lack quinone-binding proteins, *Biochim. Biophys. Acta Bioenerg.* 933 (1) (1988) 85–94.

Supporting Information

Here are provided twelve supplementary figures and one supplementary table. The first three figures demonstrate the quality of the fit for the simultaneous target analysis of eight datasets as reported in the main text and show the residual analysis. The next four figures show the full kinetic scheme used in the target analysis of the different samples for both S1 and S2. Then a figure showing the reconstructed decay associated spectra (DAS) from the target analysis as well complete table with corresponding lifetimes and assignments of these lifetimes to the different subunits of the target model. Finally the complete target analysis of the data on the chemically locked S1 to S2 transition reported in (Włodarczyk et al. 2015) with the target model from this work (and analogous figures).

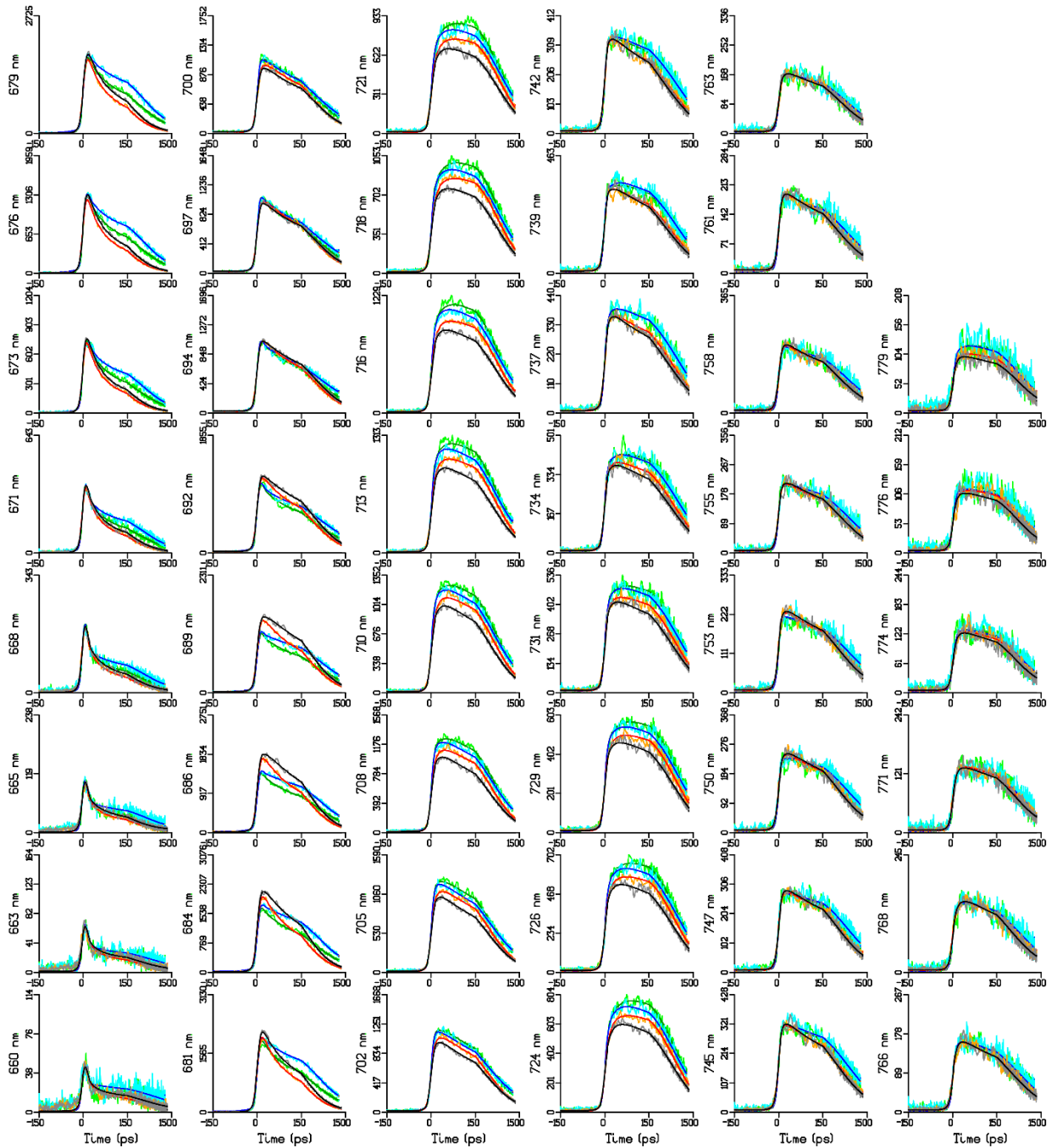


Figure S 1: Time-resolved emission (traces scaled to their maximum) at 46 wavelengths (indicated in the ordinate label) after excitation with 400 nm. Data for WT S1 & S2 shown in gray and orange, black and red lines indicate the fit after target analysis. Data for FUD7 S1 & S2 shown in cyan and light green, fit in blue and dark green respectively. Note that the time axis is linear until 150 ps, and logarithmic thereafter.

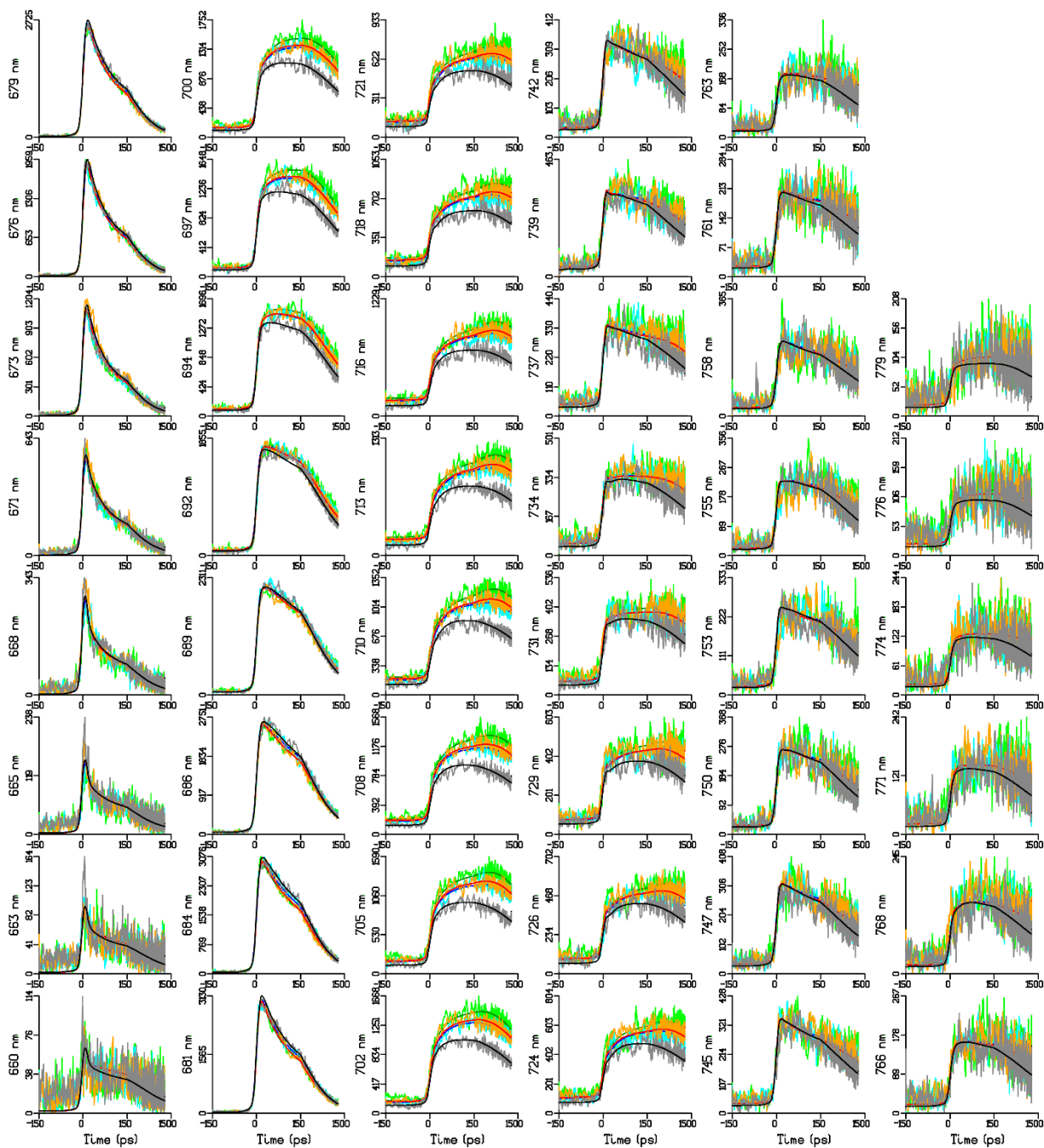


Figure S 2. Time-resolved emission (traces scaled to their maximum) at 46 wavelengths (indicated in the ordinate label) after excitation with 400 nm. Data for F15 S1 & S2 shown in gray and orange, black and red lines indicate the fit after target analysis. Data for M18 S1 & S2 shown in cyan and light green, fit in blue and dark green respectively. Note that the time axis is linear until 150 ps, and logarithmic thereafter.

In addition to visually inspecting the individual traces, it is also necessary to do a singular value decomposition (SVD) of the residual matrix to reveal possible significant structure in the residual matrix. For each of the four pairs of datasets, WT, FUD7, F15 and M18 in State 1 and State 2 the first left and right singular vector of the SVD are depicted in Figure S 3. We observe no systematic trends that would warrant adding components to the model.

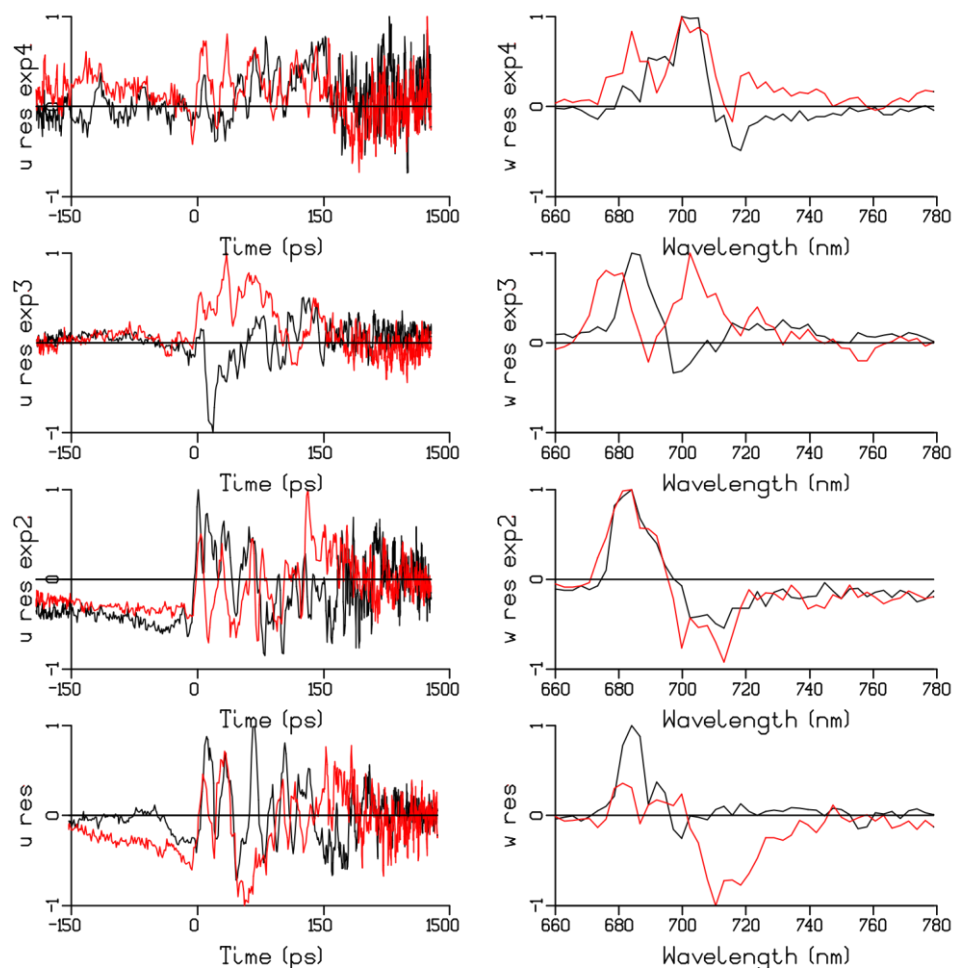


Figure S 3. The first left (u res) and right (w res) singular vectors resulting from a singular value decomposition of the residual matrix for the 8 simultaneously analyzed datasets. S1 is depicted in black, S2 in red. From bottom to top are shown WT, FUD7, F15 and M18. Note that the time axis is linear until 150 ps, and logarithmic thereafter.

Full kinetic schemes for each sample in the simultaneous analysis of all eight datasets.

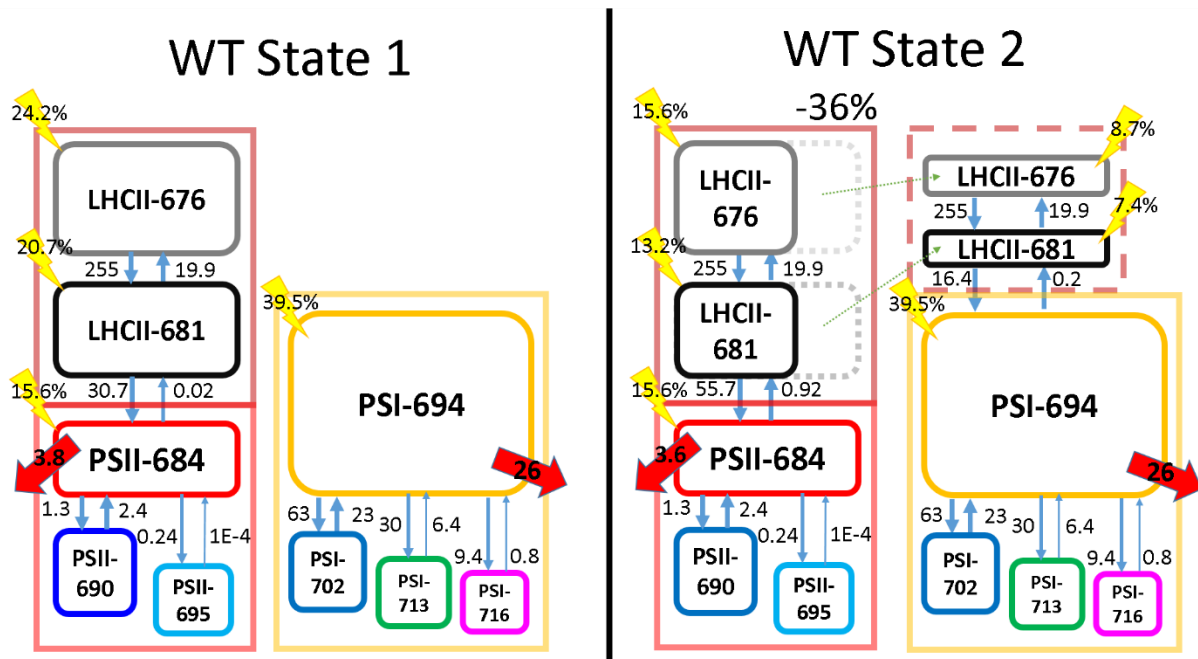


Figure S 4. Full kinetic scheme used in the target analysis of the WT datasets in S1 and S2. Here we combine the compartmental schemes from Figure 2 and Figure 4 with the information from Table 1, thus providing a detailed view of Figure 6. The relative input in each compartment is given as percentage of the total, all rates are given in /ns. The dashed green arrows in State 2 indicate the state transition, and the relative amount of LHCII involved (36%) is written on top.

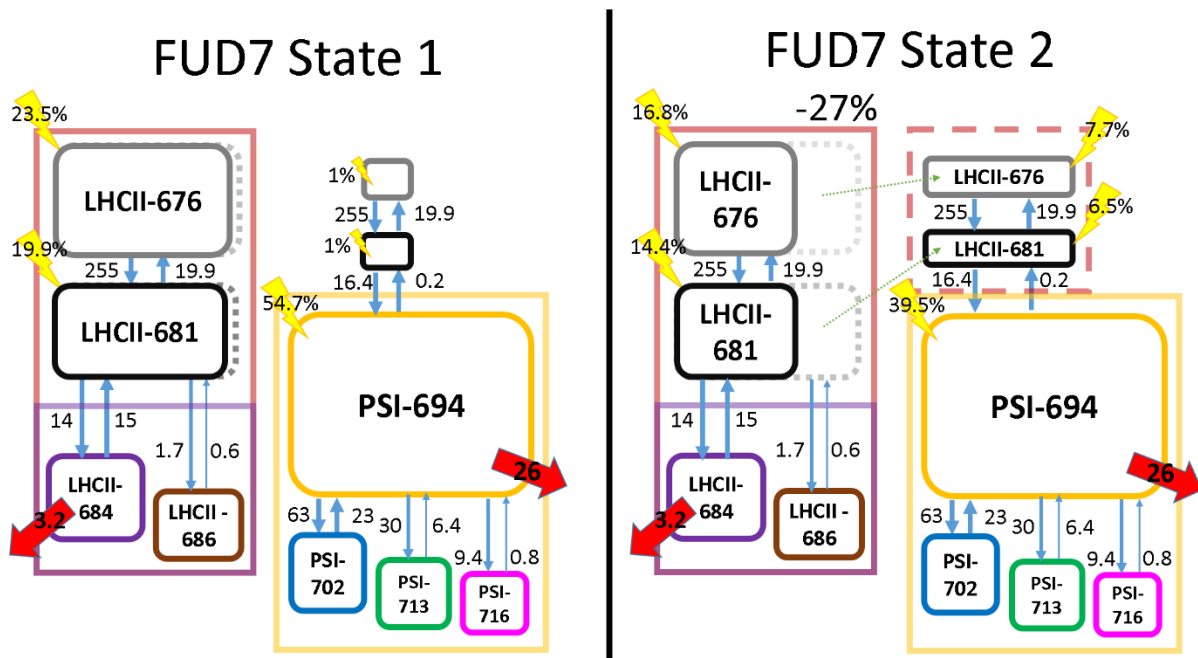


Figure S 5. Full kinetic scheme used in the target analysis of the FUD7 datasets in S1 and S2. Here we combine the compartmental schemes from Figure 3 and Figure 4 with the information from Table 1. Further information, see the caption of Figure S 4.

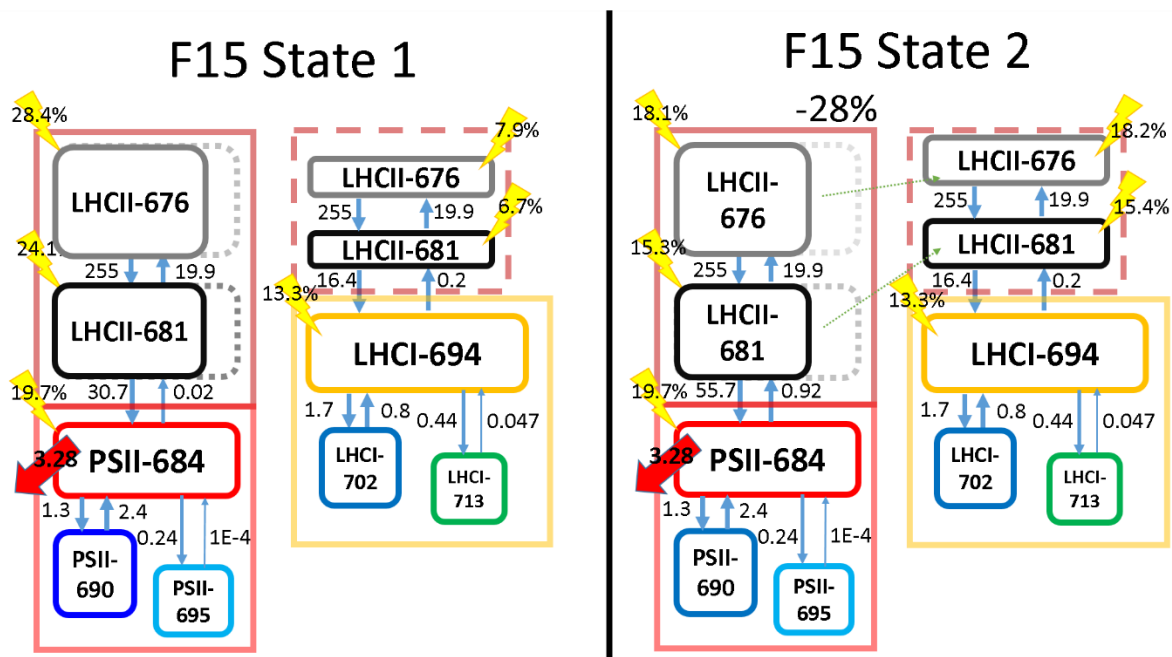


Figure S 6. Full kinetic scheme used in the target analysis of the F15 datasets in S1 and S2. Here we combine the compartmental schemes from Figure 2 and Figure 5 with the information from Table 1. Further information, see the caption of Figure S 4.

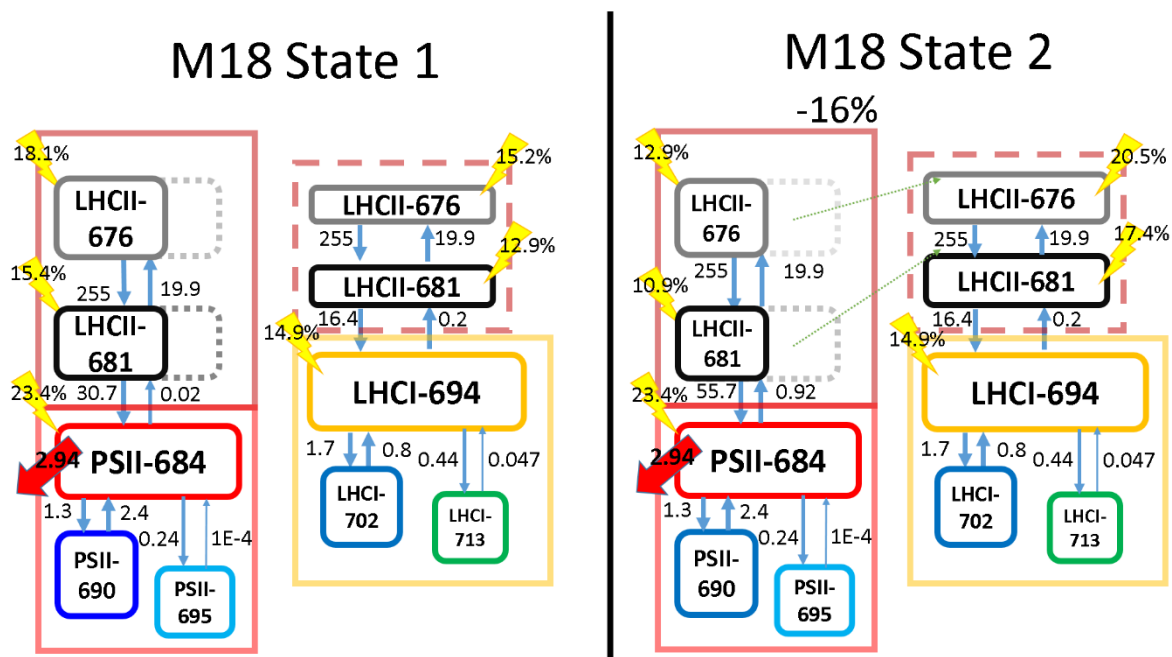


Figure S 7. Full kinetic scheme used in the target analysis of the M18 datasets in S1 and S2. Here we combine the compartmental schemes from Figure 2 and Figure 5 with the information from Table 1. Further information, see the caption of Figure S 4.

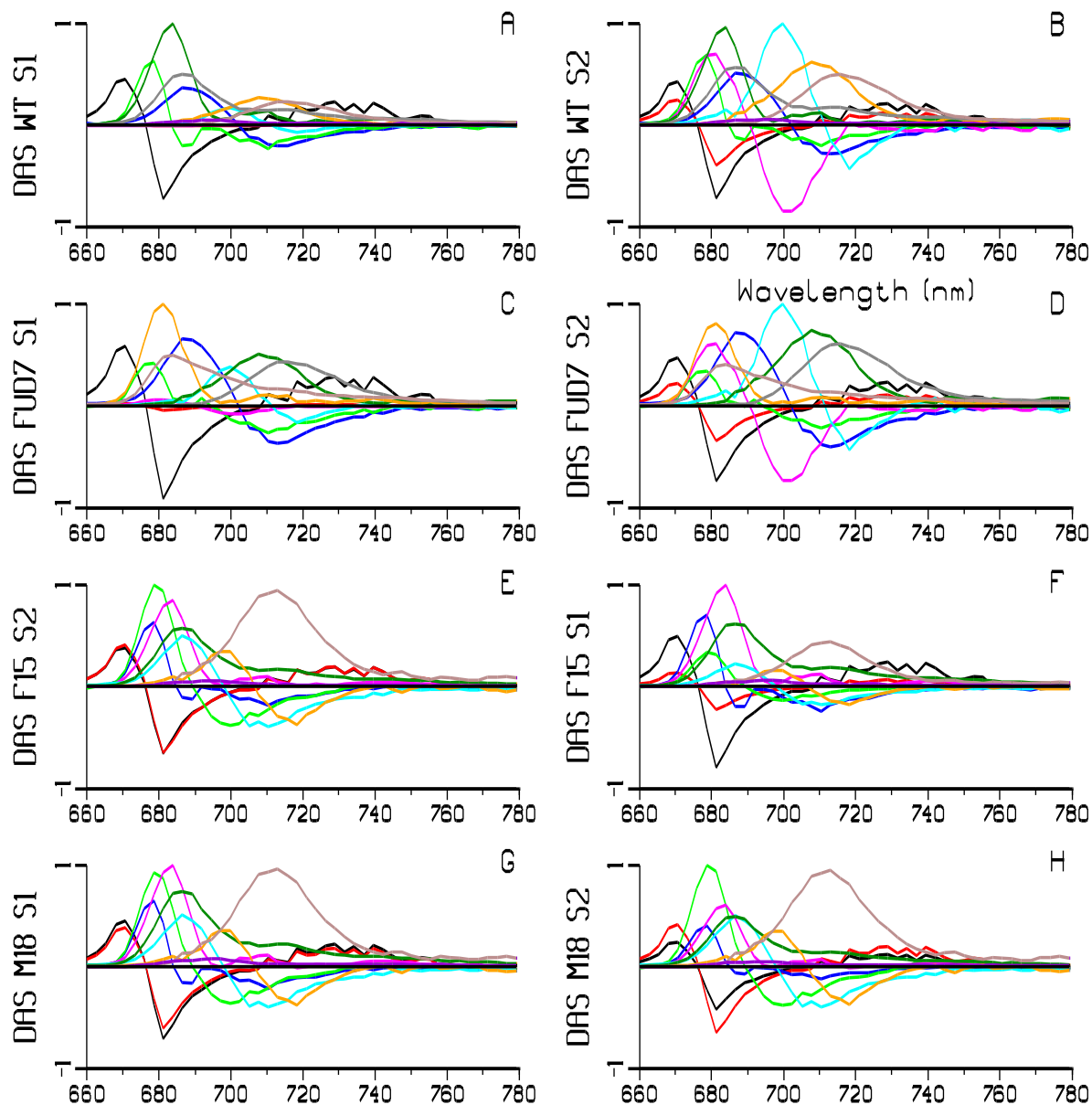


Figure S 8 Reconstructed DAS from the target analysis. Color key and lifetimes (in ps) indicated in Table S 1.

Table S 1. Lifetimes in picoseconds of the DAS of Figure S 8, with samples and their composition indicated.

	τ_1	τ_2	τ_3	τ_4	τ_5	τ_6	τ_7	τ_8	τ_9	τ_{10}	τ_{11}	sample composition	
	Black	Red	Blue	Green	Magenta	Cyan	Darkgr	Orange	Grey	Brown	Purple		
WT S1	3.61	3.62	7.0	35.2	64.8	75.8	161	303	576	1155	4998	LHCII-LHCI-PSI	LHCII-PSII
WT S2	3.57	3.62	7.0	19.3	64.8	75.8	168	303	590	1155	4998	LHCII-LHCI-PSI	LHCII-PSII
FUD7 S1	3.62	3.62	7.0	32.2	64.8	75.8	303	374	1155	2087		LHCII-LHCI-PSI	LHCII+
FUD7 S2	3.62	3.62	7.0	32.2	64.8	75.8	303	374	1155	2087		LHCII-LHCI-PSI	LHCII+
F15 S1	3.61	3.62	35.2	64.1	173	308	615	2049	3126	3128	4998	LHCII-LHCI	LHCII-PSII
F15 S2	3.57	3.62	19.3	64.1	175	308	617	2049	3126	3128	4998	LHCII-LHCI	LHCII-PSII
M18 S1	3.61	3.62	35.2	64.1	181	308	649	2049	3126	3128	4998	LHCII-LHCI	LHCII-PSII
M18 S2	3.57	3.62	19.3	64.1	183	308	652	2049	3126	3128	4998	LHCII-LHCI	LHCII-PSII

Target analysis of the chemically locked S1 to S2 transition from (Wlodarczyk et al. 2015)

Chlamydomonas reinhardtii wild-type (WT) which came from the lab of Prof. Jean-David Rochaix was used. The growth conditions, treatments and measurement protocols have been described in more detail before (Wlodarczyk et al. 2015). Briefly, the cells were grown under constant illumination with $25 \mu\text{mol photons m}^{-2} \text{s}^{-1}$ PAR in Tris-acetate-phosphate (TAP) medium at 25°C with constant mixing (170 rpm) on an incubator shaker (Minitron, INFORS HT). Cells for measurements were harvested in a mid-logarithmic phase of growth ($\text{OD}_{750} \approx 0.7$). A batch of cells was then prepared in S1 by strongly aerating them in the dark for 90 min in the presence of $0.1 \mu\text{M}$ staurosporine, a kinase inhibitor which prevents phosphorylation of LHCII (Takahashi et al. 2006). This chemically locked state 1 was denoted as **S1c**. For state 2, cells were incubated 45 min under anaerobic conditions in the dark in the presence of sodium fluoride (0.1 M) in order to inhibit dephosphorylation of LHCII (Takahashi et al. 2006). This chemically locked state 2 was denoted as **S2c**. After induction of S1 or S2, intact *C.r.* cells were instantly frozen in the presence of glycerol as cryoprotectant (65% v/v) in nitrogen cryostat (Oxford) and kept in this state for the duration of the measurement. The samples were measured on a synchroscan streak-camera setup described in detail elsewhere (van Stokkum et al. 2006; van Stokkum et al. 2008). The excitation pulses (**475 nm**, $\approx 100 \text{ fs}$) carried an energy per pulse of 14 nJ and were used to excite the sample with a repetition rate of 50 kHz. The resulting laser beam was focused on the sample giving a spot of $\approx 150 \mu\text{m}$ in diameter. Time-resolved emission in the window of 660 nm to 818 nm over a range of 1.5 ns with 1.5 ps step size was used for data analysis. The FWHM of the instrument response function (IRF) was found to be 14 ps. The time-resolved fluorescence of S1c and S2c were simultaneously analyzed with the same target model as presented in the main text.

For these data we present in Figure S 9 and Figure S 10 the compartmental model, concentration profiles and estimated SAS for respectively the LHCII-PSII and LHCII-LHCI-PSI supercomplex, analogous to Figure 2 and Figure 4 in the main text. In both figures the population profiles and the SAS from the main text have been added in panels D and E to facilitate visual comparison. The raw data traces overlaid with the fit shown in Figure S 11 show the satisfactory agreement of the present model with these data. However, a careful analysis of the residual matrix presented in Figure S 12 analogous to Figure S 3 does reveal a significant residual concentrated around 685 nm. This is what in the previous paper (Wlodarczyk et al. 2015) was captured by a component designated X-685 and which is now missing from the used target model because it was not necessary to fit the data reported on in the main text. Apparently, X-685 is only present after a “chemically induced” state transition. Note that the “chemically induced” state transition is larger than the “nonchemically induced” state transition, compare the relative differences between the solid and dashed lines in Figure S 9B and D and in Figure S 10B and D. This can only partly be attributed to the 475 instead of 400 nm excitation.

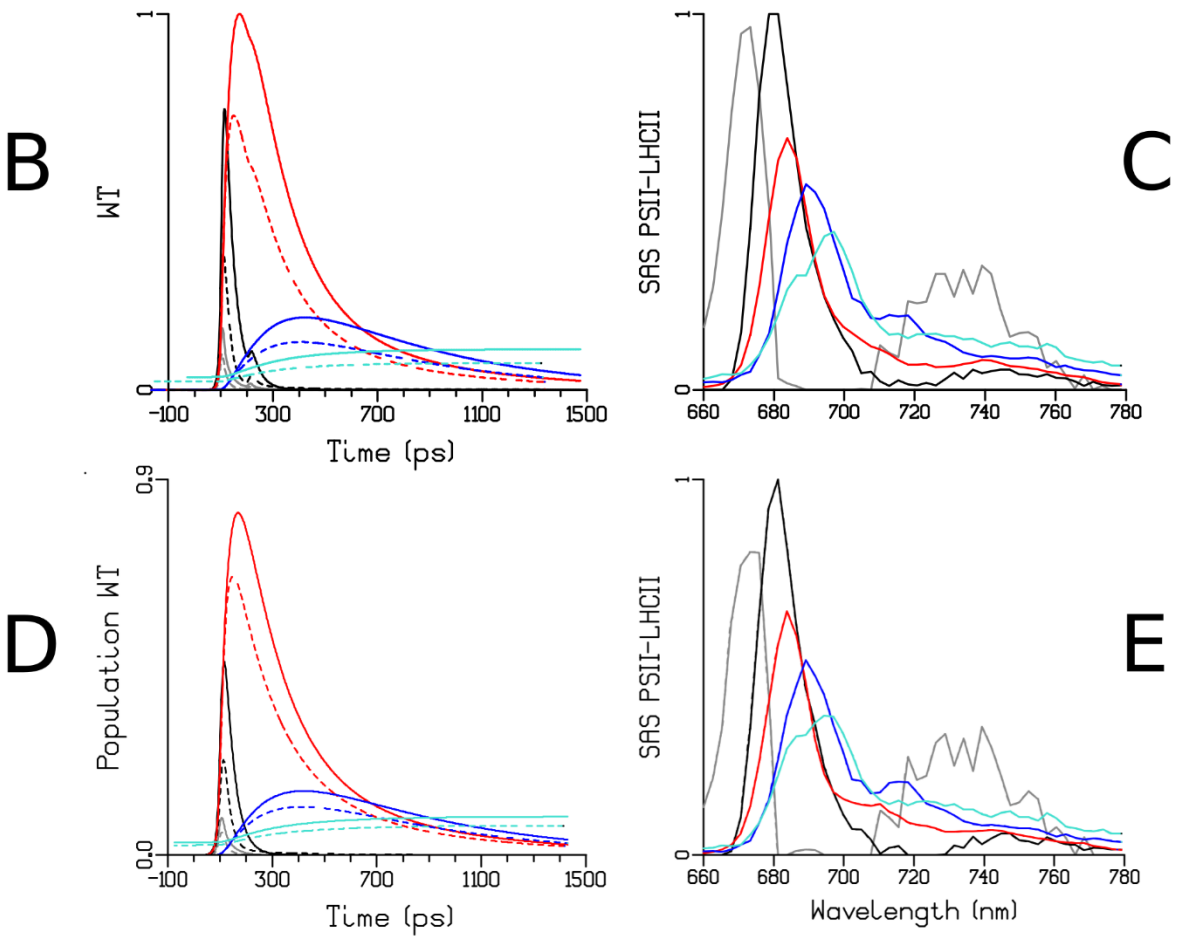
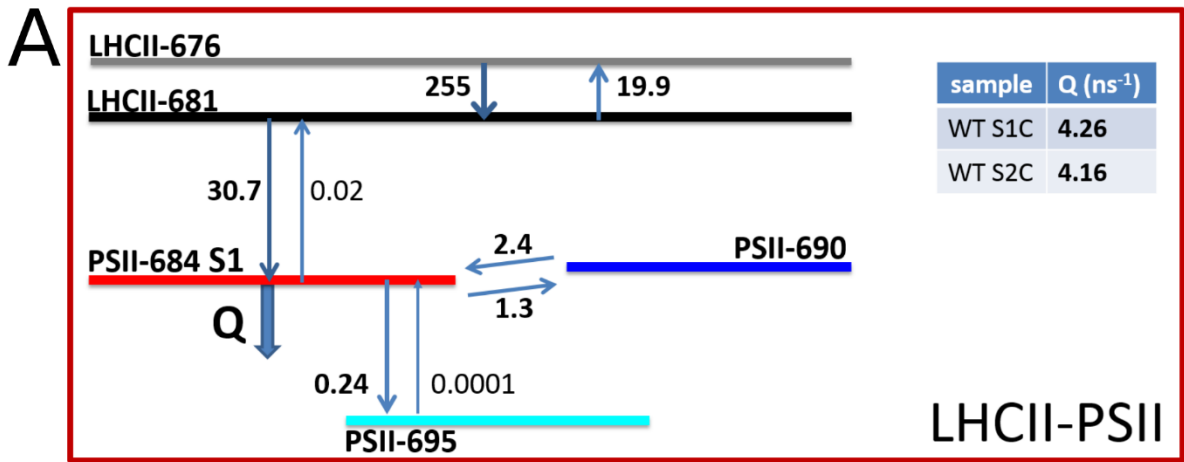


Figure S 9. Compartmental model for the LHCII-PSII supercomplex at 77 K. All rates are in ns⁻¹ and fixed to the estimated values reported in the main text, except for the variable quenching rate Q which remained a free parameter (inset table). B) Population dynamics in WT (S1c solid, S2c dashed) and C) estimated SAS for the S1c and S2c data. D) Population dynamics in WT (S1 solid, S2 dashed) and E) estimated SAS for the S1 and S2 data.

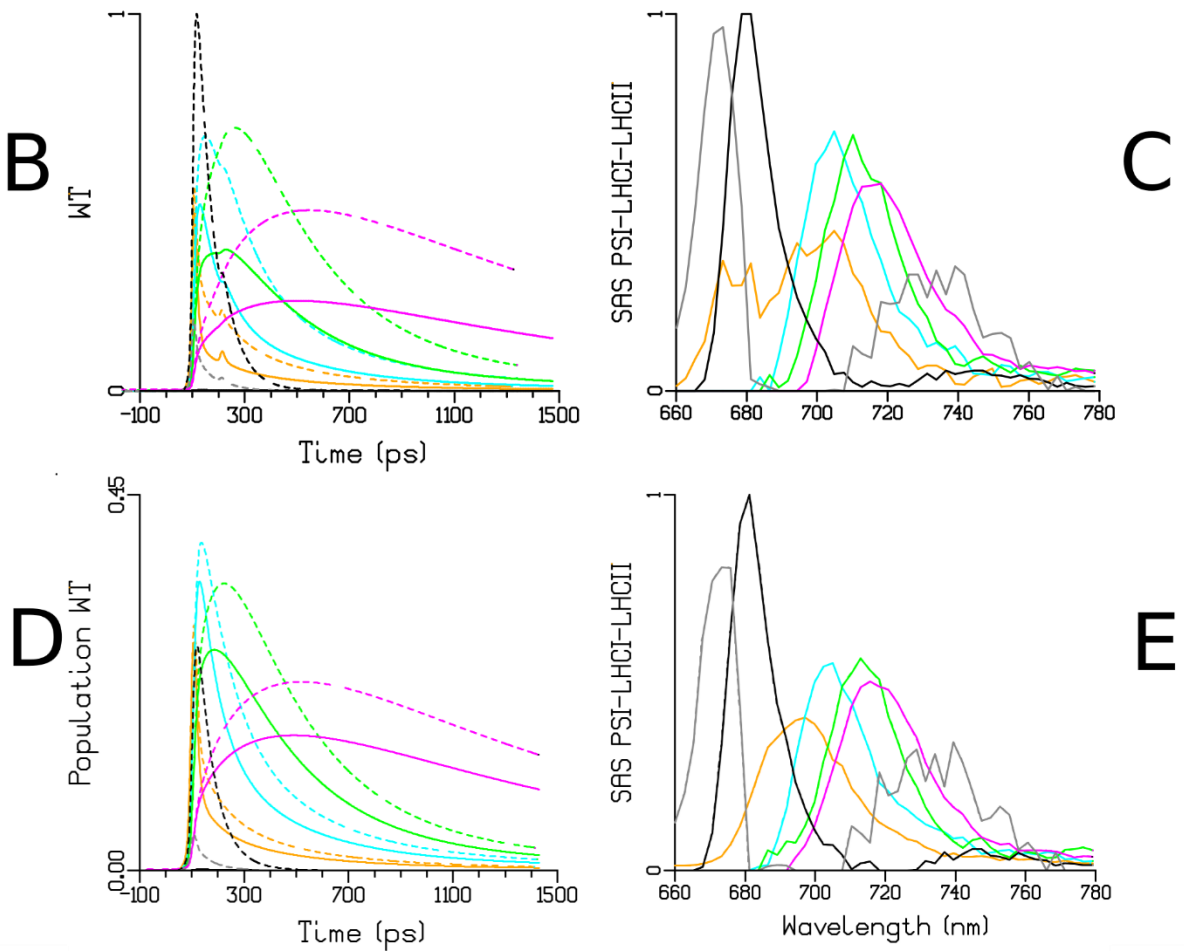
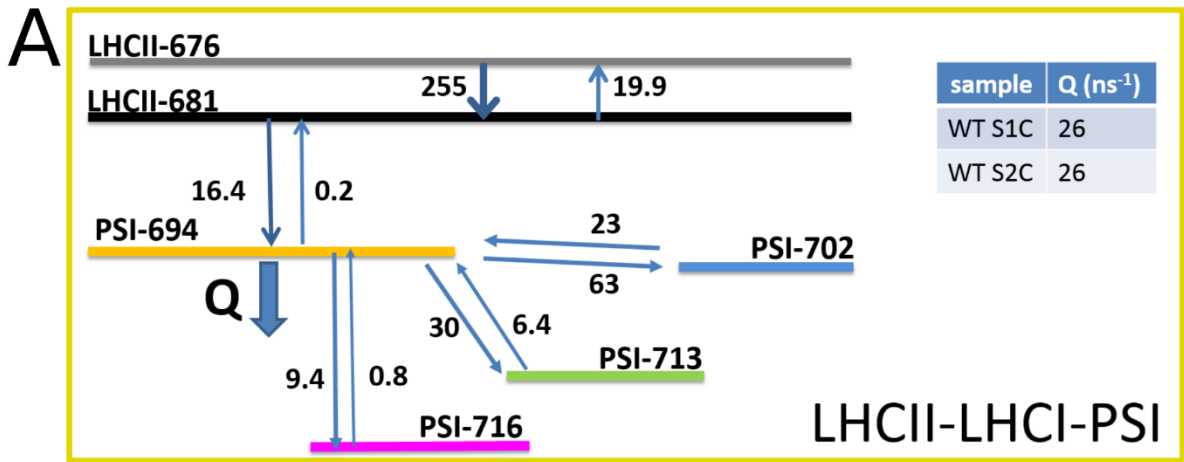


Figure S 10. A) Compartmental model for the LHCII-LHCI-PSI subunit at 77K. All rates are in ns⁻¹ and fixed to the estimated values reported in the main text. B) Population dynamics in WT (S1c solid, S2c dashed) and C) estimated SAS for the S1c and S2c data. D) Population dynamics in WT (S1 solid, S2 dashed) and E) estimated SAS for the S1 and S2 data.

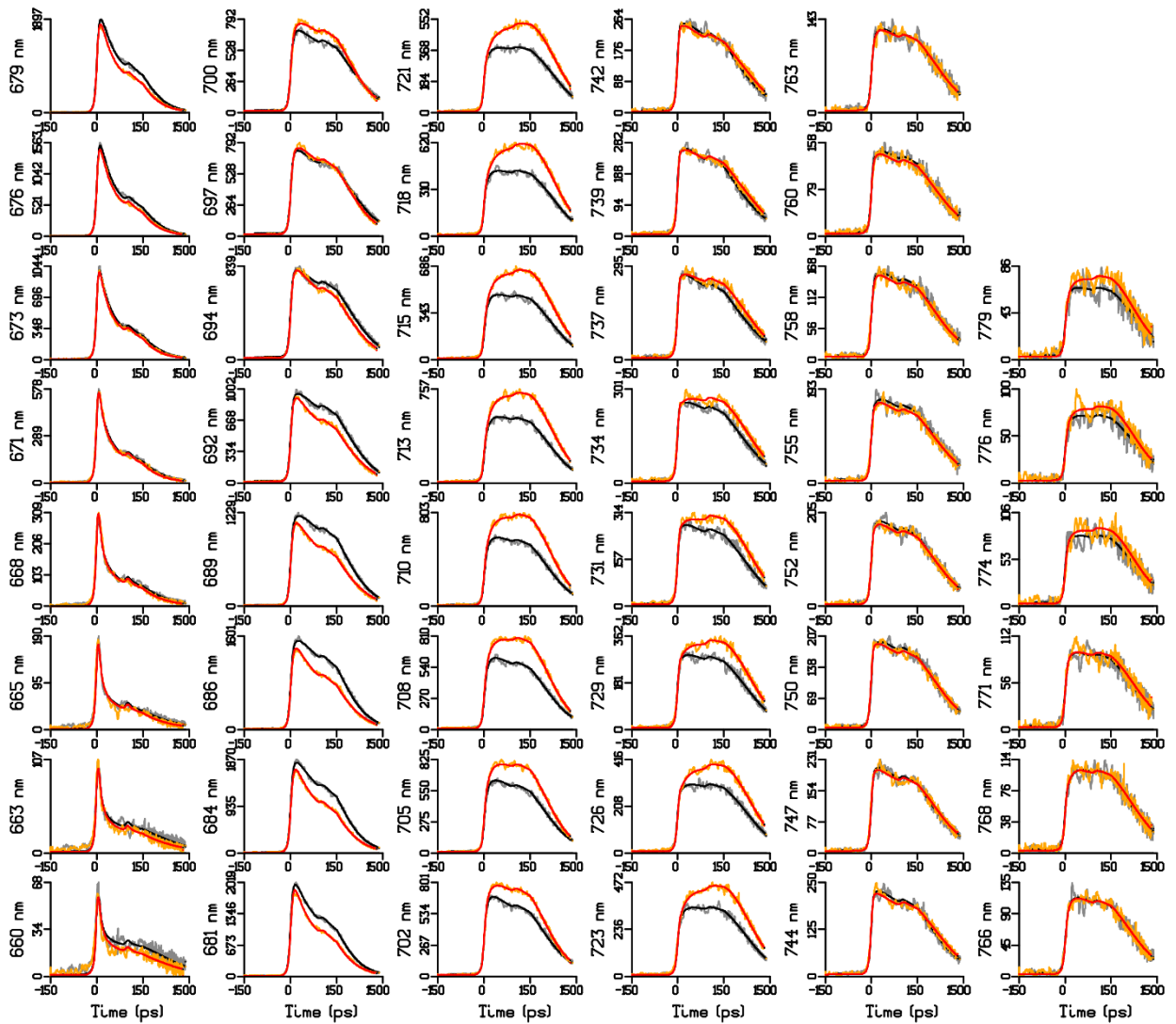


Figure S 11. Time-resolved emission (traces scaled to their maximum) at 46 wavelengths (indicated in the ordinate label) after 475 nm excitation of intact, instantly frozen C.r. cells poised in S1 or in S2 (chemically locked) as described in (Włodarczyk et al. 2015); see also Figure S3 and Figure S4 of that reference. In gray and orange is shown the data for WT S1c & S2c, black and red lines indicate the fit after target analysis using the model reported in this paper (see Figure S 9, Figure S 10). Note that the time axis is linear until 150 ps, and logarithmic thereafter.

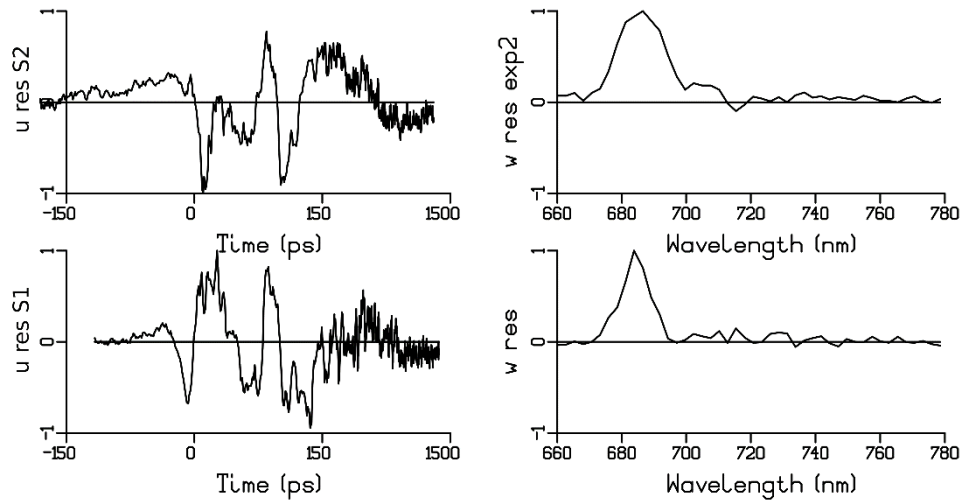


Figure S 12. The first left and right singular vectors resulting from a singular value decomposition of the residual matrix for the two simultaneously analyzed datasets WT S1c & S2c shown in Figure S 11. S1c is depicted in the bottom row, S2c in the top row. Note that the time axis is linear until 150 ps, and logarithmic thereafter.

Although the quality of the fit in Figure S 11 is good, a clear trend in the residual singular vectors in Figure S 12 can be observed corresponding to emission centered around 685 nm (see the right singular vector w_{res}), in particular in S2c, where the left singular vector u_{res} is large and positive from 120-300 ps. Previously this was assigned to a component designated X-685 (Włodarczyk et al. 2015). No such component was necessary to fit the WT data reported in the present paper and therefore X-685 was not included in the model, but as it was present in the (Włodarczyk et al. 2015) data, it shows up here in the residual analysis.